

# Synthesis, Molecular Modeling Study, and Quantum-Chemical-Based Investigations of Isoindoline-1,3-diones as Antimycobacterial Agents

Iqrar Ahmad, Rahul H. Pawara, Rukaiyya T. Girase, Asama Y. Pathan, Vilas R. Jagatap, Nisheeth Desai, Yusuf Oloruntoyin Ayipo, Sanjay J. Surana, and Harun Patel\*



Cite This: *ACS Omega* 2022, 7, 21820–21844



Read Online

ACCESS |



Metrics & More

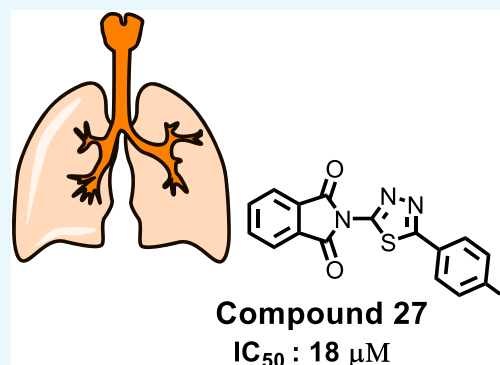


Article Recommendations



Supporting Information

**ABSTRACT:** The condensation of phthalic anhydride afforded structurally modified isoindoline-1,3-dione derivatives with selected amino-containing compounds. The title compounds (2–30) have been characterized by thin-layer chromatography (TLC), infrared spectroscopy,  $^1\text{H}$  and  $^{13}\text{C}$  NMR spectroscopy, and mass spectroscopy. All of the compounds were assessed for their antimycobacterial activity toward the H37Rv strain by a dual read-out assay method. Among the synthesized compounds, compound 27 possessed a significant  $\text{IC}_{50}$  of 18  $\mu\text{M}$ , making it the most potent compound of the series. The InhA inhibitory ( $\text{IC}_{50}$ ) activity of compound 27 was 8.65  $\mu\text{M}$  in comparison to Triclosan (1.32  $\mu\text{M}$ ). Computational studies like density functional theory (DFT) study, molecular docking, and dynamic simulation studies illustrated the reactivity and stability of the synthesized compounds as InhA inhibitors. A quantum-mechanics-based DFT study was carried out to investigate the molecular and electronic properties, reactivities, and nature of bonding present in the synthesized compounds and theoretical vibrational (IR) and isotropic value ( $^1\text{H}$  and  $^{13}\text{C}$  NMR) calculations.



## 1. INTRODUCTION

Tuberculosis (TB), caused by *Mycobacterium tuberculosis* (Mtb), is one of the most fatal infectious diseases burdening the world.<sup>1</sup> The WHO has recently updated its data on TB deaths, which shows that 1.5 million people (including 214,000 people with human immunodeficiency virus (HIV)) died from TB in 2020. TB is the 13th leading cause of mortality worldwide and the second leading infectious killer after COVID-19 (above HIV/acquired immunodeficiency syndrome (AIDS)). In 2020, there are estimated 10 million new cases of tuberculosis (TB) worldwide, including 3.3 million women, 5.6 million men, and 1.1 million children.<sup>1–3</sup> The 30 most high-burden countries in 2020 will account for 86% of new TB cases. Eight countries make up two-thirds of the total, with India leading the pack, followed by China, Indonesia, the Philippines, Pakistan, Nigeria, Bangladesh, and South Africa. Globally, the TB rate is declining at a rate of about 2% per year, and it declined by 11% between 2015 and 2020.

In the 1960s, the use of pyrazinamide and rifampicin led to a radical transformation of antimycobacterial therapy.<sup>4</sup> Combined with isoniazid, ethambutol, and/or streptomycin, it has led to short-course chemotherapy (SCC), which reduces the time of treatment from 18 to 6 months.<sup>5–8</sup> The prolonged course of treatment leads many patients to stop taking the medication after their symptoms disappear. By stopping the medication before the infection has cleared up, the bacteria can

develop resistance to the antibiotic, potentially leading to multidrug-resistant (MDR) infection.<sup>5–8</sup> HIV co-infection further complicates the ability to treat TB, increasing resistance to treatment and the transmission rates and death due to TB.<sup>8</sup> According to these findings, there is an urgent need to develop an antitubercular treatment that is less toxic and more effective than the current first- and second-line antitubercular drugs. A subunit of isoindoline-1,3-dione is an important drug candidate having a variety of biological activities against diseases including cancer, leprosy, inflammation, AIDS, cyclooxygenase (COX) inhibitors, multiple myeloma, and antidepressants.<sup>9</sup> Structure–activity relationships (SAR) of metabolites and analogues of thalidomide have shown that the isoindoline-1,3-dione ring system plays an essential role in the drug's pharmacophore.<sup>10</sup> Isoindoline-1,3-diones possess planar aromatic ring and hydrophobicity; therefore, interaction of these drugs with different biologically active targets constitutes the basis for the evaluation of their biological activity.<sup>11</sup> Due to

Received: April 1, 2022

Accepted: May 19, 2022

Published: June 10, 2022



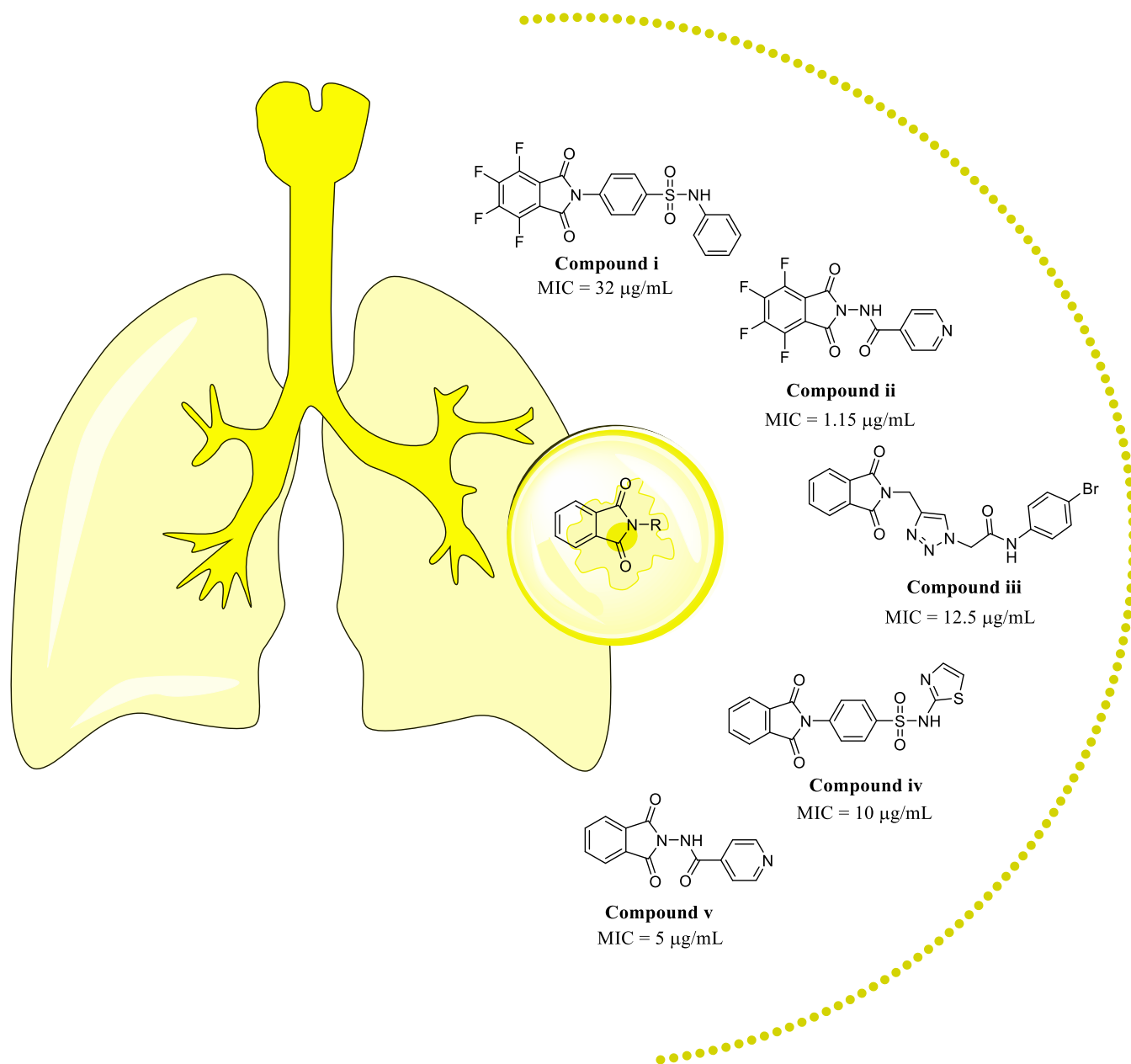


**Figure 1.** Reported isoindoline-1,3-dione derivatives.

their planar aromatic ring and hydrophobicity, isoindoline-1,3-diones interact with a variety of biologically active target molecules. Thus, the interaction between these drugs and their biological targets provides the basis for the evaluation of their biological activity.<sup>12</sup> The minimal inhibitory concentrations (MICs) of some of these derivatives with an N-substituted isoindoline-1,3-dione moiety are comparable to those of clinically used antibiotics.<sup>12</sup>

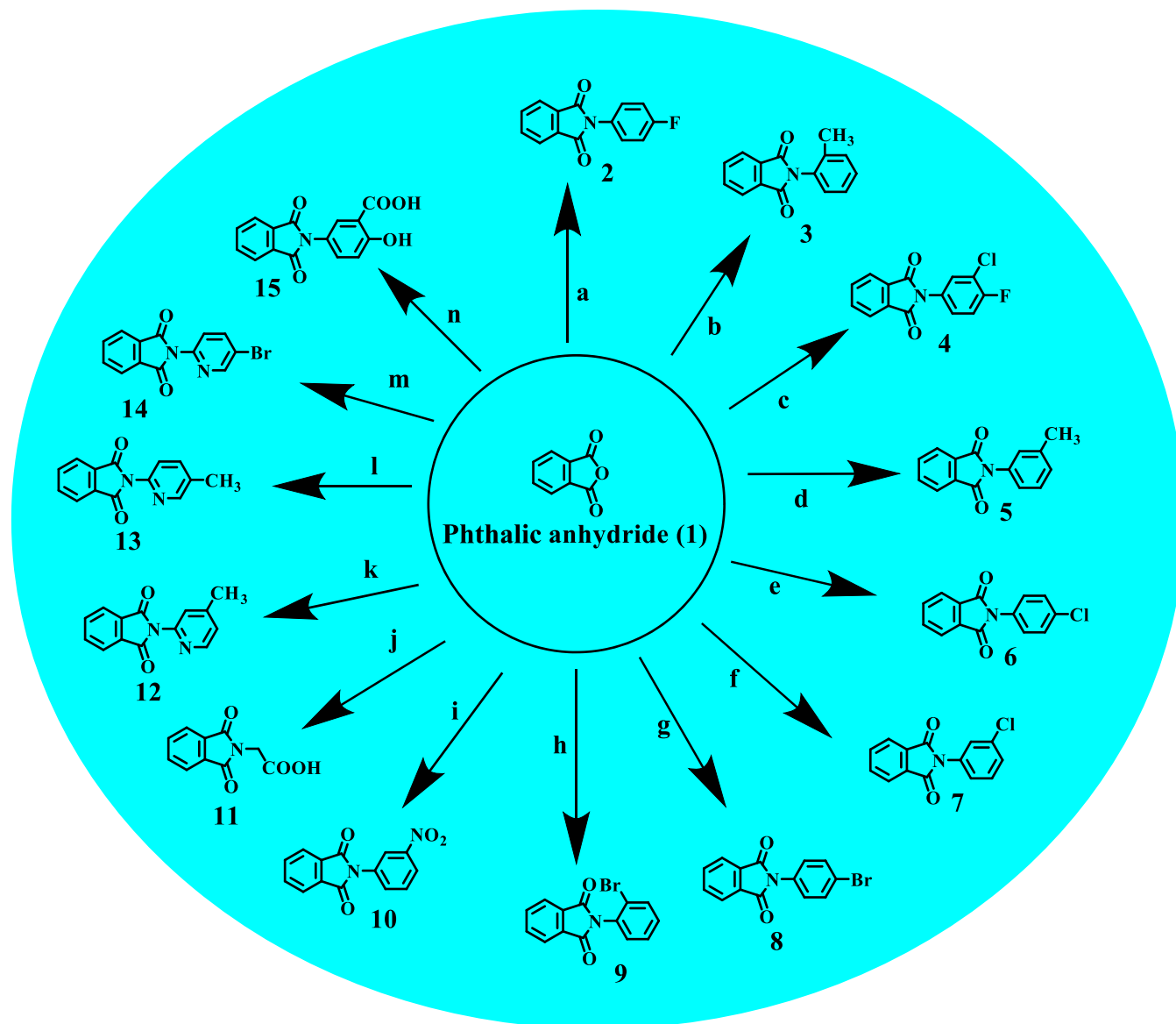
Akgün et al. reported the sulfonamido-fused isoindoline-1,3-dione derivative **i** with an MIC of 32  $\mu\text{g/mL}$  against the H<sub>37</sub>Ra strain.<sup>9</sup> In an article by Elumalai et al., they described an isoniazid-fused compound **ii** with an MIC of 1.15  $\mu\text{g/mL}$  against H37Rv.<sup>13</sup> In their study, Phatak et al. examined the antimycobacterial activity of an isoindoline-1,3-dione bearing 1,2,3-triazole (compound **iii**) with an MIC of 12.5  $\mu\text{g/mL}$ .<sup>14</sup> As reported by Paraiso et al., sulfonamido-clubbed isoindoline-1,3-dione derivatives **iv** have an MIC of 10  $\mu\text{g/mL}$  against the

*M. tuberculosis* H<sub>37</sub>Rv strain.<sup>15</sup> Several nonfluorinated derivatives of isoniazide (**v**) have been synthesized by Santos et al. (MIC: 5  $\mu\text{g/mL}$ ) (Figure 1).<sup>16</sup>

Inspired by the above literature, in the current research work, we have reported the synthesis, spectroscopic study, molecular modeling, and quantum-mechanics-based investigation of the isoindoline-1,3-dione derivatives as an antimycobacterial agent.

## 2. RESULT AND DISCUSSION

**2.1. Chemistry.** The isoindoline-1,3-dione derivatives (2–30) were prepared by condensing an equimolar quantity of phthalic anhydride and primary amino group containing alicyclic compounds in 50–75 mL glacial acetic acid in an equimolar quantity (Schemes 1 and 2). After pouring the content into the ice, a solid precipitated out, which was filtered and recrystallized from ethanol (60–80% yields), and the

Scheme 1<sup>a</sup>

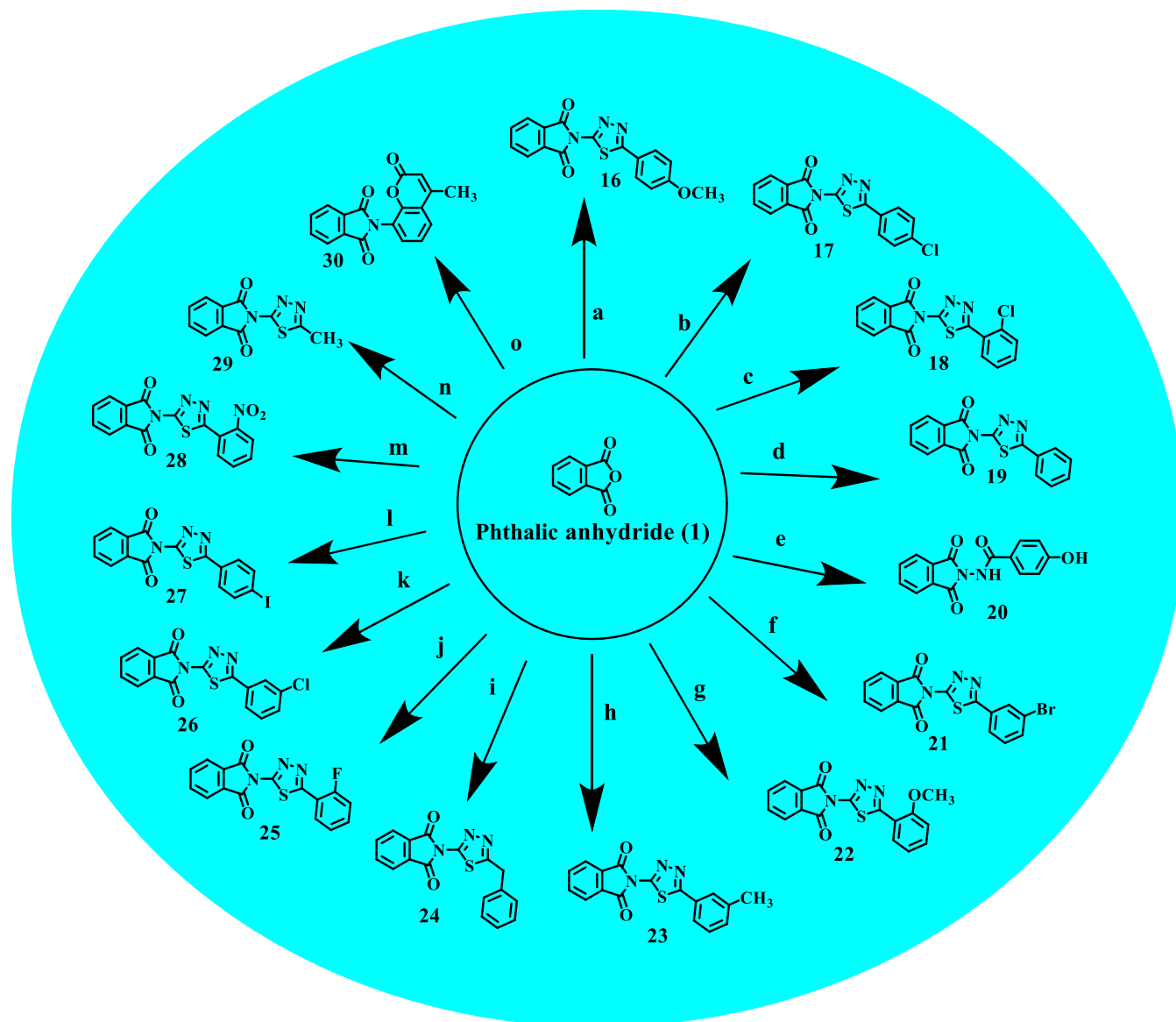
<sup>a</sup>Reagents and conditions: 0.1 mol of the primary amino group containing alicyclic compound, 0.1 mol of phthalic anhydride in 50–75 mL of glacial acetic acid, reflux for 3 h; (a) 4-fluoroaniline, (b) 2-methylaniline, (c) 3-chloro-4-fluoroaniline, (d) 3-methylaniline, (e) 4-chloroaniline, (f) 3-chloroaniline, (g) 4-bromoaniline, (h) 2-bromoaniline, (i) 3-nitroaniline, (j) glycine, (k) 4-methylpyridin-2-amine, (l) 5-methylpyridin-2-amine, (m) 5-bromopyridin-2-amine, (n) 5-amino-2-hydroxybenzoic acid.

compounds were purified by flash chromatography. Thin-layer chromatography (TLC) was used to verify the purity of synthesized compounds, and spectroscopic data were used to identify their structures. The IR spectra of compounds 2–30 displayed the characteristic band indicating the carbonyl group of the imide isoindoline-1,3-dione ring, ranging from 1699 to 1779  $\text{cm}^{-1}$ . The  $^1\text{H}$  NMR spectra of compounds 2–30 showed multiple signals corresponding to resonances of isoindoline-1,3-dione protons at 6.45–8.48  $\delta$  ppm. The  $^{13}\text{C}$  NMR and mass data further confirmed the synthesis of the title compounds 2–30. The lipophilicity values ( $\text{Log}P$ ) of the synthesized compounds (2–30) were calculated using CHEMDRAW ultra-14.0.

The synthesis of the isoindoline-1,3-dione derivatives (2–30) was successfully carried out from phthalic anhydride and different primary amino-containing heterocycles with 95–

100% purity. Purification of the compounds was carried out using flash chromatography and verified by liquid chromatography–mass spectrometry (LCMS).

**2.2. Theoretical and Experimental Spectral Correlation.** The use of IR and NMR ( $^1\text{H}$  and  $^{13}\text{C}$ ) spectroscopy, nowadays coupled with theoretical computations, is proving to be an effective tool for analyzing the vibrational and chemical shifts within molecules.<sup>17</sup> The vibrational spectra, chemical shifts, and simulated outcomes can help to distinguish vibrational modes, chemical shifts (isotropic value), and structural features of the synthesized compounds.<sup>18</sup> Using density functional theory (DFT)/B3LYP methods with the B3LYP/6-311\*\* basis set, we examined the vibrational spectra and chemical shift (isotropic value).<sup>17,18</sup> First, conformational search of compound 14 was first performed using the OPLS-2005 method. Consequently, the conformers were reoptimized

Scheme 2<sup>a</sup>

<sup>a</sup>Reagents and conditions: 0.1 mol of the primary amino group containing alicyclic compound, 0.1 mol of phthalic anhydride in 50–75 mL of glacial acetic acid, reflux for 3 h; (a) 5-(4-methoxyphenyl)-1,3,4-thiadiazol-2-amine, (b) 5-(4-chlorophenyl)-1,3,4-thiadiazol-2-amine, (c) 5-(2-chlorophenyl)-1,3,4-thiadiazol-2-amine, (d) 5-phenyl-1,3,4-thiadiazol-2-amine, (e) 5-(4-methoxyphenyl)-1,3,4-thiadiazol-2-amine, (f) 5-(3-bromophenyl)-1,3,4-thiadiazol-2-amine, (g) 5-(3-methylphenyl)-1,3,4-thiadiazol-2-amine, (h) 5-(3-methylphenyl)-1,3,4-thiadiazol-2-amine, (i) 5-benzyl-1,3,4-thiadiazol-2-amine, (j) 5-(2-fluorophenyl)-1,3,4-thiadiazol-2-amine, (k) 5-(3-chlorophenyl)-1,3,4-thiadiazol-2-amine, (l) 5-(4-iodophenyl)-1,3,4-thiadiazol-2-amine, (m) 5-(2-nitrophenyl)-1,3,4-thiadiazol-2-amine, (n) 5-methyl-1,3,4-thiadiazol-2-amine, (o) 8-amino-4-methyl-2H-chromen-2-one.

by applying DFT at the B3LYP/6-311\*\* level. The geometry optimized parameters of compound 14 are given in Table 1.

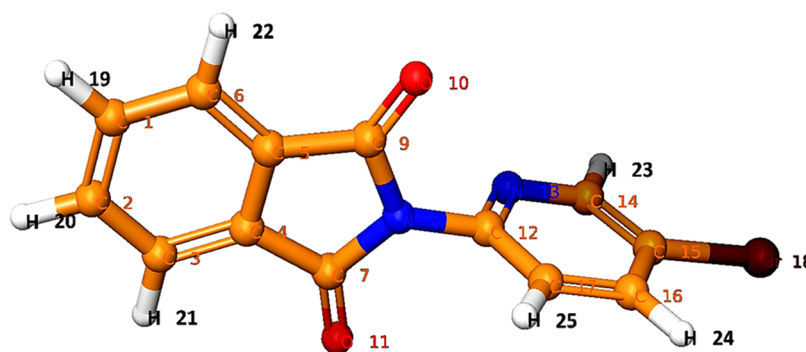
**2.2.1. Vibrational Analysis (IR Spectral Analysis).** IR spectra were recorded for the solid substances using the KBr press pellet technique in the region between 4000 and 400  $\text{cm}^{-1}$  with 40 number of scans on a Shimadzu FTIR-8400S at a resolution of 4 Hz. The calculated vibrational wavenumbers and IR intensities of compound 14 are provided in Table 2 and Figures 2 and 3. The linear correlations between calculated and assessed data have been obtained by the DFT/B3LYP method and are illustrated by eq 1.

$$\nu_{\text{calc}} = 0.999\nu_{\text{expt}} - 5.875 \quad (R^2 = 0.9991) \quad (1)$$

As the DFT calculated vibrational wavenumbers were higher than those calculated experimentally, they were scaled down by the scaling factors 0.958 and 0.983 for the wavenumbers in the range of 4000–1700  $\text{cm}^{-1}$  and lower than 1700  $\text{cm}^{-1}$ , respectively.<sup>19</sup>

We compared the scaled theoretical values with the experimental values for compound 14. The CH vibrations are a common vibrational frequency observed in IR spectra. Unsaturated hydrocarbons have vibrational frequencies ranging from 3100 to 3000  $\text{cm}^{-1}$ . Experimental aromatic CH stretching was observed at 3064.99  $\text{cm}^{-1}$ , and a calculated peak was observed at 3032.00  $\text{cm}^{-1}$  for compound 14. It is easy to recognize the stretching vibrational absorption of C=O since

Table 1. Geometry-Optimized Structure of Compound 14 by DFT



bond angles (deg)		torsional angles (deg)		bond lengths (Å)
C6–C1–C2: 121.101621	H23–C14–N13: 117.071275	C1–C2–C3–C4: –0.123433	C7–N8–C9–O10: –179.025033	C1–C2: 1.401747
H19–C1–C2: 119.318463	H23–C14–C15: 120.702746	C1–C2–C3–H21: –179.918978	C7–N8–C12–N13: 85.109609	C1–C6: 1.400602
H19–C1–C6: 119.579865	C16–C15–C14: 119.899225	C1–C6–C5–C4: –0.124082	C7–N8–C12–C17: –94.890391	C1–H19: 1.086312
C3–C2–C1: 121.101621	Br18–C15–C14: 119.57376	C1–C6–C5–C9: 179.776645	N8–C12–N13–C14: 180.000000	C2–C3: 1.400602
H20–C2–C1: 119.318463	Br18–C15–C16: 120.527014	C2–C1–C6–C5: 0.123433	N8–C12–C17–C16: 179.999999	C2–H20: 1.086312
H20–C2–C3: 119.579865	C17–C16–C15: 117.701529	C2–C1–C6–H22: 179.918978	N8–C12–C17–H25: 0.000001	C3–C4: 1.386955
C4–C3–C2: 117.303383	H24–C16–C15: 120.967860	C2–C3–C4–C5: 0.124082	C9–C5–C6–H22: –0.021522	C3–H21: 1.085525
H21–C3–C2: 121.955182	H24–C16–C17: 121.330612	C2–C3–C4–C7: –179.776645	C9–N8–C7–O11: 179.025033	C4–C5: 1.395452
H21–C3–C4: 120.741115	C16–C17–C12: 118.254907	C3–C2–C1–C6: 0.000000	C9–N8–C12–N13: –85.109609	C4–C7: 1.490906
C5–C4–C3: 121.594877	H25–C17–C12: 120.290287	C3–C2–C1–H19: 179.917540	C9–N8–C12–C17: 94.890391	C5–C6: 1.386955
C7–C4–C3: 129.710583	H25–C17–C16: 121.45480	C3–C4–C5–C6: 0.000000	O10–C9–N8–C12: –7.844467	C5–C9: 1.490906
C7–C4–C5: 108.694481		C3–C4–C5–C9: –179.919378	O11–C7–N8–C12: 7.844467	C6–H22: 1.085525
C6–C5–C4: 121.594877		C3–C4–C7–N8: –179.191936	C12–N13–C14–C15: 0.000000	C7–N8: 1.414388
C9–C5–C4: 108.694481		C3–C4–C7–O11: 0.224911	C12–N13–C14–H23: 180.000000	C7–O11: 1.210985
C9–C5–C6: 129.710583		C4–C3–C2–H20: 179.793894	C12–C17–C16–C15: 0.000000	N8–C9: 1.414388
C5–C6–C1: 117.303383		C4–C5–C6–H22: –179.922250	C12–C17–C16–H24: 179.999999	N8–C12: 1.423335
H22–C6–C1: 121.955182		C4–C5–C9–N8: –0.897331	N13–C12–C17–C16: 0.000000	C9–O10: 1.210985
H22–C6–C5: 120.741115		C4–C5–C9–O10: 179.685821	N13–C12–C17–H25: 180.000000	C12–N13: 1.332308
N8–C7–C4: 105.075084		C4–C7–N8–C9: –1.528816	N13–C14–C15–C16: 0.000000	C12–C17: 1.394047
O11–C7–C4: 129.387418		C4–C7–N8–C12: –172.709383	N13–C14–C15–Br18: 180.000000	N13–C14: 1.333632
O11–C7–N8: 125.534776		C5–C4–C3–H21: 179.922250	C14–N13–C12–C17: 0.000001	C14–C15: 1.397358
C9–N8–C7: 112.437750		C5–C4–C7–N8: 0.897331	C14–C15–C16–C17: 0.000000	C14–H23: 1.086646
C12–N8–C7: 123.466902		C5–C4–C7–O11: –179.685821	C14–C15–C16–H24: 180.000000	C15–C16: 1.392428
C12–N8–C9: 123.466902		C5–C6–C1–H19: –179.79389	C15–C16–C17–H25: 180.000000	C15–Br18: 1.90764
N8–C9–C5: 105.075084		C5–C9–N8–C7: 1.528816	C16–C15–C14–H23: 180.000000	C16–C17: 1.392395
O10–C9–C5: 129.387418		C5–C9–N8–C12: 172.70938	C17–C16–C15–Br18: 180.000000	C16–H24: 1.084458
O10–C9–N8: 125.534776		C6–C1–C2–H20: –179.917540	Br18–C15–C14–H23: 0.000000	C17–H25: 1.084341
N13–C12–N8: 116.130169		C6–C5–C4–C7: 179.919378	Br18–C15–C16–H24: 0.000001	
C17–C12–N8: 119.725519		C6–C5–C9–N8: 179.191936	H19–C1–C2–H20: 0.000000	
C17–C12–N13: 124.1443		C6–C5–C9–O10: –0.22491	H19–C1–C6–H22: 0.001651	
C14–N13–C12: 117.7740		C7–C4–C3–H21: 0.021522	H20–C2–C3–H21: –0.001651	
C15–C14–N13: 122.2259		C7–C4–C5–C9: 0.000000	H24–C16–C17–H25: 0.000000	

it usually appears in the region of  $\sim 1700\text{ cm}^{-1}$  with a sharp, distinct peak.

The experimental peak of the C=O peak at  $1718.63\text{ cm}^{-1}$  and the theoretical scaled peak was observed at  $1729.00$ . The C–N (m–s) and C=N (m–s) peaks are generally observed between  $1350\text{--}1000$  and  $1690\text{--}1640\text{ cm}^{-1}$ . Experimentally, C–N and C=N peaks are observed at  $1357.93$  and  $1570.11\text{ cm}^{-1}$  and at  $1360.49$  and  $1572.22\text{ cm}^{-1}$  in the simulated spectrum, respectively. The bromide usually appears at  $<667\text{ cm}^{-1}$  in IR. Practically, it appeared at  $665.46\text{ cm}^{-1}$  and theoretically, by quantum mechanics, at  $646.70\text{ cm}^{-1}$ .

**2.2.2.  $^1\text{H}$  NMR Spectral Analysis.** At ambient temperature,  $^1\text{H}$  NMR and  $^{13}\text{C}$  NMR spectra were recorded on a Bruker Avance-II 400 NMR spectrometer operating at 400 MHz. Chemical shifts were calculated and reported in  $\delta$  ppm in comparison to the internal standard tetramethylsilane (TMS)

(Table 3 and Figures 4 and 5).  $^1\text{H}$  NMR spectra provide information about peak shapes, chemical shifts, sources of hydrogen atoms, coupling constants, etc. Aromatic hydrogen atoms tend to appear in high-field regions, and aliphatic hydrogen atoms appear in low-field regions; with an increased electron cloud density, electronegative groups can increase the chemical shift.<sup>17–20</sup>

The linear correlation between calculated and observed data was found for compound 14 by the DFT/B3LYP method and is explained by eq 2.

$$\delta_{\text{calc}} = 0.987\delta_{\text{expt}} - 0.0183 \quad (R^2 = 0.9552) \quad (2)$$

As shown in Table 3, H21 and H22 of the isoindoline-1,3-dione ring of compound 14 are in the same chemical environment and should appear as doublet of doublet (dd). In the simulation study, they had an isotropic shielding value of

Table 2. Experimental and Calculated Wavenumbers (cm<sup>-1</sup>) for Compound 14

mode	experimental IR	calculated IR by B3LYP/6-311**		mode	experimental IR	calculated IR by B3LYP/6-311**	
		unscaled	scaled			unscaled	scaled
1		33.07	32.51	36		1171.60	1151.69
2		46.69	45.90	37		1200.45	1180.04
3		79.62	78.27	38		1219.70	1198.96
4		124.43	122.31	39		1245.64	1224.46
5		143.21	140.78	40		1286.82	1264.95
6		169.39	166.51	41		1306.73	1284.51
7		177.07	174.06	42		1364.00	1340.81
8		235.44	231.43	43	1357.93	1384.02	1360.49
9		288.57	283.66	44		1439.47	1415.00
10		291.24	286.29	45		1444.20	1419.65
11		348.94	343.01	46		1460.58	1435.75
12		369.19	362.92	47	1465.95	1512.64	1486.93
13		376.14	369.74	48		1538.27	1512.12
14		444.47	436.91	49	1570.11	1599.41	1572.22
15		461.42	453.57	50		1626.21	1598.56
16		506.24	497.63	51		1644.88	1616.92
17		553.41	544.00	52		1650.97	1622.90
18		558.33	548.84	53		1682.28	1653.68
19		578.97	569.13	54		1692.26	1663.49
20		638.34	627.48	55		1721.25	1648.95
21	665.46	657.89	646.70	56		1725.96	1653.47
22	715.61	722.32	710.04	57		1738.93	1665.90
23		737.00	724.47	58		1757.39	1683.58
24		755.47	742.62	59	1718.63	1804.81	1729.00
25	786.98	770.95	757.85	60		1809.16	1733.18
26	835.21	840.12	825.84	61		1873.55	1794.86
27	883.43	856.11	841.56	62		1934.41	1853.16
28		927.50	911.73	63		3144.55	3012.48
29		986.32	969.55	64		3146.35	3014.21
30	1006.88	1030.97	1013.45	65		3150.33	3018.02
31		1052.82	1034.93	66		3151.00	3018.66
32	1072.46	1100.22	1081.51	67		3153.79	3021.33
33		1103.17	1084.42	68		3158.79	3026.12
34		1132.09	1112.84	69	3064.99	3164.93	3032.00
35		1139.92	1120.54	70			

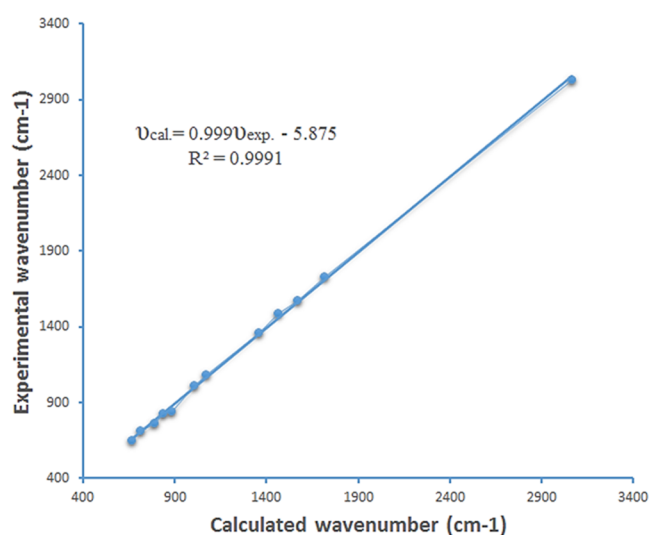


Figure 2. Linear regression between experimental and calculated wavenumbers for compound 14.

23.63 and the calculated <sup>1</sup>H NMR chemical shift relative to TMS was found to be 8.01 δ ppm. The average experimental

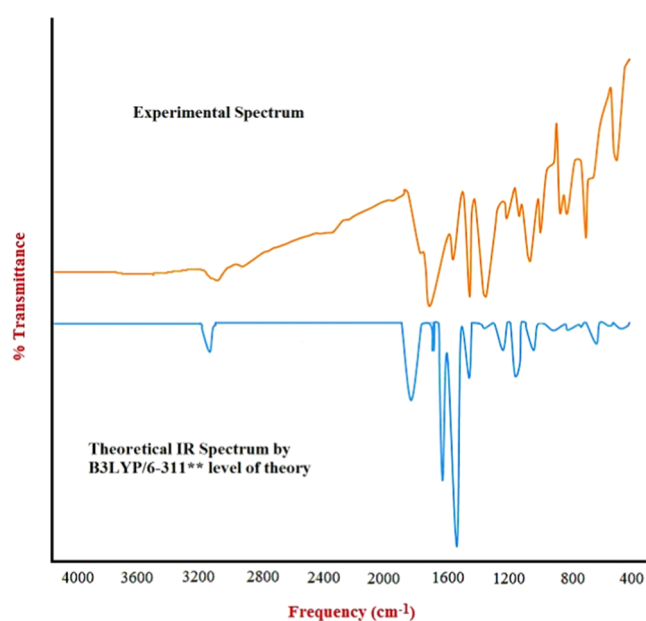
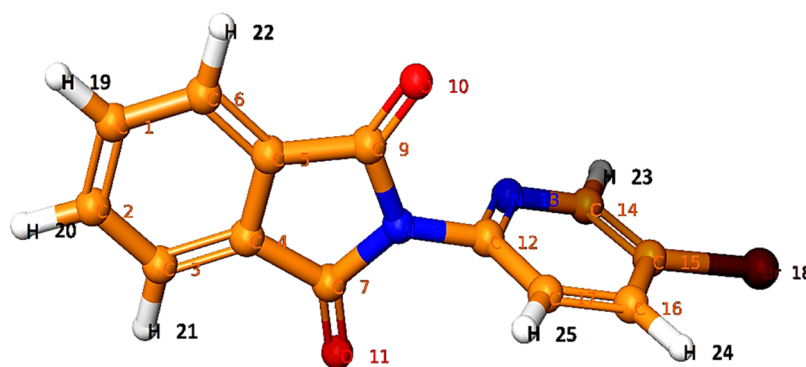
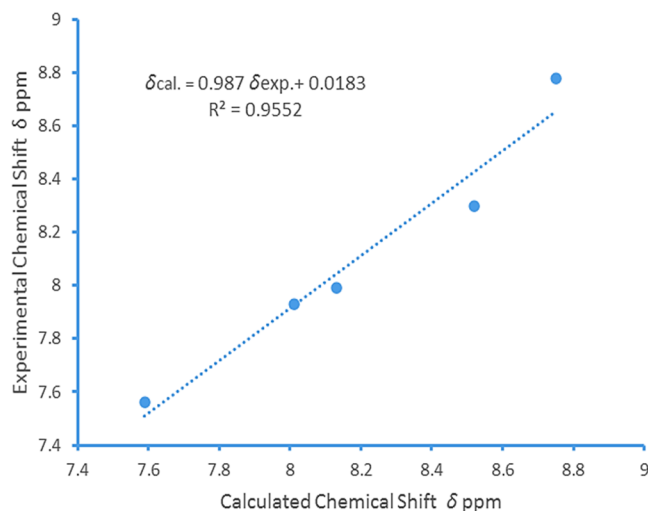


Figure 3. Experimental and theoretical IR spectra of compound 14.

Table 3. Experimental and Calculated  $^1\text{H}$  NMR Spectra of Compound 14

label	isotropic shielding	calculated $^1\text{H}$ NMR chemical shift relative to TMS ( $\delta$ ppm)	experimental chemical shift (multiplets) ( $\delta$ ppm)	average chemical shift ( $\delta$ ppm)
H19 and H20	23.51	8.13	7.9873–8.0087	7.99
H21 and H22	23.63	8.01	7.9204–7.9419	7.93
H23	22.89	8.75	8.7906–8.7847	8.78
H24	23.12	8.52	8.2838–8.3113	8.3
H25	24.05	7.59	7.5794–7.5582	7.56



**Figure 4.** Analysis of the linear relationship between experimental and calculated chemical shifts ( $^1\text{H}$  NMR) for compound 14.

chemical shift was observed at 7.93  $\delta$  ppm (dd). Similarly, H19 and H20 were having similar chemical environment (isotropic value: 23.51) and their calculated chemical shift was observed at 8.13  $\delta$  ppm and practical average chemical shift as dd observed at 7.99  $\delta$  ppm. The meta coupled H23 of 4-bromo pyridinyl of compound 14 appeared at 8.78–8.79  $\delta$  ppm (average: 8.78  $\delta$  ppm), and in quantum simulation, it appeared at 8.75  $\delta$  ppm with an isotropic value of 22.89.

A sharp doublet of H25 appeared at 7.55–7.57  $\delta$  ppm (average: 7.56  $\delta$  ppm), and a theoretical calculated chemical shift appeared at 7.59  $\delta$  ppm. A double-notched doublet of pyridinyl proton H24 was observed at 8.28–8.31  $\delta$  ppm (average: 8.3  $\delta$  ppm), and the calculated  $^1\text{H}$  NMR chemical shift relative to TMS appeared at 8.52  $\delta$  ppm (Figure 5).

**2.2.3.  $^{13}\text{C}$  NMR Spectral Analysis.** The  $^{13}\text{C}$  chemical shift of carbon is determined to a large extent by its hybrid orbital states. Generally,  $\text{sp}^3$  hybrid carbons have a resonance in the high field,  $\text{sp}^2$  hybrid carbons have one in the low field, and  $\text{sp}$  hybrid carbons resonate in between them. Using TMS as an internal standard substance,  $\delta$  values of  $\text{sp}^3$  carbon range

between 0 and 60 ppm,  $\text{sp}^2$  hybrid carbon is in between 100 and 150 ppm, and the range of  $\delta$  values of  $\text{sp}$  hybrid carbon is 60–95 ppm.<sup>17–23</sup>

Besides induction and conjugation effects, the variation in electron cloud density outside the carbon nucleus can also affect chemical shifts. This results in a shift of the resonance absorption peak in high and low fields.<sup>17,18</sup> The Bruker Avance-II 400 NMR spectrometer operating at 400 MHz was used to record  $^{13}\text{C}$  NMR spectra, and chemical shifts were measured compared to the TMS (Table 4 and Figures 6 and 7). The characteristic carbonyl carbon (C7 and C9) of the isoindoline-1,3-dione ring of compound 14 appeared at 166.04  $\delta$  ppm (calculated: 174.35  $\delta$  ppm). Other aromatic carbons of compound 14 are observed between 119.98 and 150.08  $\delta$  ppm. A significant linear correlation has been observed between calculated and observed chemical shift data for  $^{13}\text{C}$  NMR (Figure 6) and is described by eq 3.

$$\delta_{\text{calc}} = 0.8517\delta_{\text{exp}} + 16.262 \quad (R^2 = 0.9216) \quad (3)$$

**2.3. Antimycobacterial Activity and Structure–Activity Relationship (SAR).** Newly synthesized compounds have been evaluated for their antimycobacterial activity using a dual read-out (OD590 and fluorescence) assay procedure to determine the MIC against the Mtb H37Rv strain.<sup>24–26</sup> Results of the antimycobacterial activity are shown in Table 5. The series of the synthesized isoindoline-1,3-diones (2–30) can be broadly divided into substituted aniline derivatives (2–15) and substituted 1,3,4-thiadiazol derivatives (16–19, 21–29) and have an  $\text{IC}_{50}$  value of 18–197  $\mu\text{M}$  against *M. tuberculosis*. Structural relationship suggested that the substituted 1,3,4-thiadiazols are more potent than the substituted anilines at the second position of the 2-isoindoline-1,3-dione [compound 27 ( $\text{IC}_{50}$ : 18  $\mu\text{M}$ ); compound 6 ( $\text{IC}_{50}$ : 28  $\mu\text{M}$ )]. Among the halo-phenyl-substituted 1,3,4-thiadiazols at the second position, iodophenyl [compound 27 ( $\text{IC}_{50}$ : 18  $\mu\text{M}$ )] was more potent compared to the chloro [compound 26 ( $\text{IC}_{50}$ : 80  $\mu\text{M}$ )], bromo [compound 21 ( $\text{IC}_{50}$ : 100  $\mu\text{M}$ )], and fluorophenyl [compound 25 ( $\text{IC}_{50}$ : 133  $\mu\text{M}$ )]. Among the anilines, 4-chloro aniline (4-chloro phenyl) has shown significant antimycobacterial activity ( $\text{IC}_{50}$ : 28  $\mu\text{M}$ ) compared

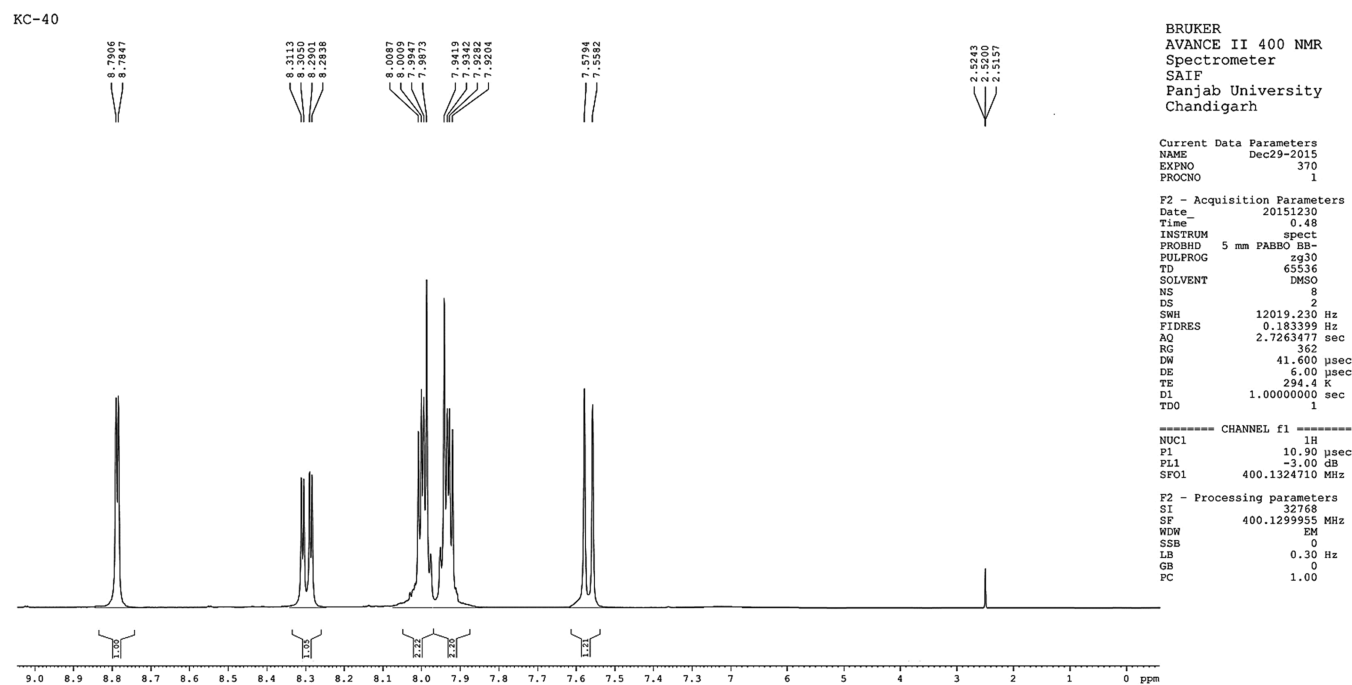
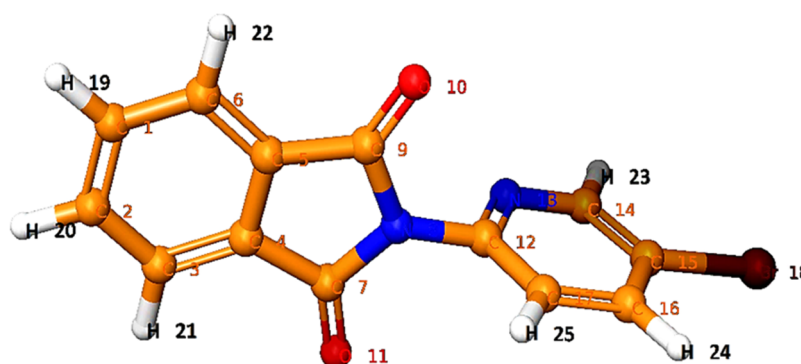


Figure 5.  $^1\text{H}$  NMR spectrum of compound 14.

Table 4. Experimental and Theoretical Calculated  $^{13}\text{C}$  NMR Spectra of Compound 14



label	isotropic shielding	calculated $^{13}\text{C}$ NMR chemical shift relative to TMS ( $\delta$ ppm)	experimental chemical shift ( $\delta$ ppm)
C1 and C2	63.13	134.73	134.98
C3 and C6	70.58	126.79	123.70
C4 and C5	60.06	138.01	131.26
C7 and C9	25.99	174.35	166.04
C12	44.18	154.95	141.20
C14	42.72	156.5	150.08
C15	73.1	124.7	119.98
C16	56.45	141.85	144.76
C17	69.73	127.69	124.42

to other anilines. It was expected that pyridine-substituted 2-isoxindolin-1,3-diones (compounds 12, 13, and 14) would show significant antimycobacterial activity, but practically, they have demonstrated only moderate antimycobacterial activity [compound 14 ( $\text{IC}_{50}$ : 90  $\mu\text{M}$ ); compound 12 ( $\text{IC}_{50}$ : 148  $\mu\text{M}$ ); compound 13 ( $\text{IC}_{50}$ : 160  $\mu\text{M}$ )] (Figure 8).

**2.4. In Vitro Cytotoxicity Evaluation.** The cytotoxic effects of potent compounds were determined by assessing THP-1 cell viability after 3 days in the presence of test compounds. Table 5 shows the cytotoxicity data of compounds 5–8 and 27. All of the tested compounds had an  $\text{IC}_{50}$  value greater than 150  $\mu\text{M}$ .<sup>24–26</sup>

**2.5. InhA Inhibitory Activity.** To determine the InhA inhibitory activity of potent compound 27, an enzyme assay was carried (Table 5). The assay was carried out utilizing 2-*trans*-dodecenoyl-CoA as a substrate, and the % inhibition was measured taking into consideration the conversion of NADH into its oxidized form  $\text{NAD}^+$  at 340 nm. Triclosan, a well-known InhA inhibitor, has been used as a reference. The  $\text{IC}_{50}$  value of potent compound 27 was found to be 8.65  $\mu\text{M}$  compared to Triclosan (1.32  $\mu\text{M}$ ).

**2.6. Docking Study.** Molecular modeling was used to investigate how the synthesized compounds bind to the active site of 2-*trans*-enoyl acyl carrier protein reductase (InhA, PDB



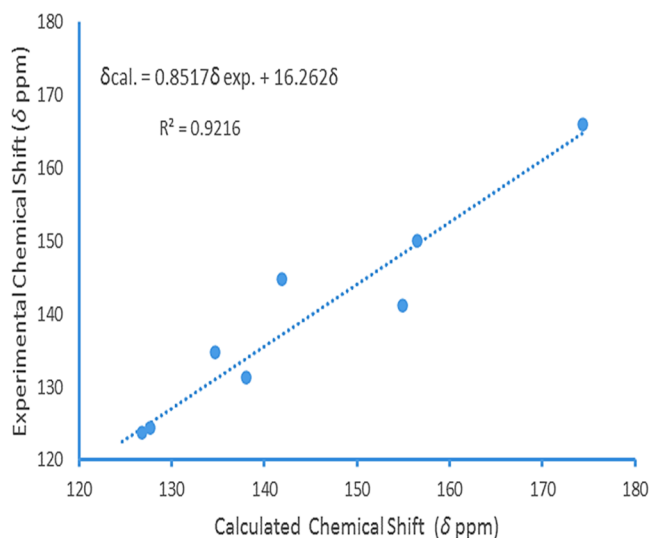
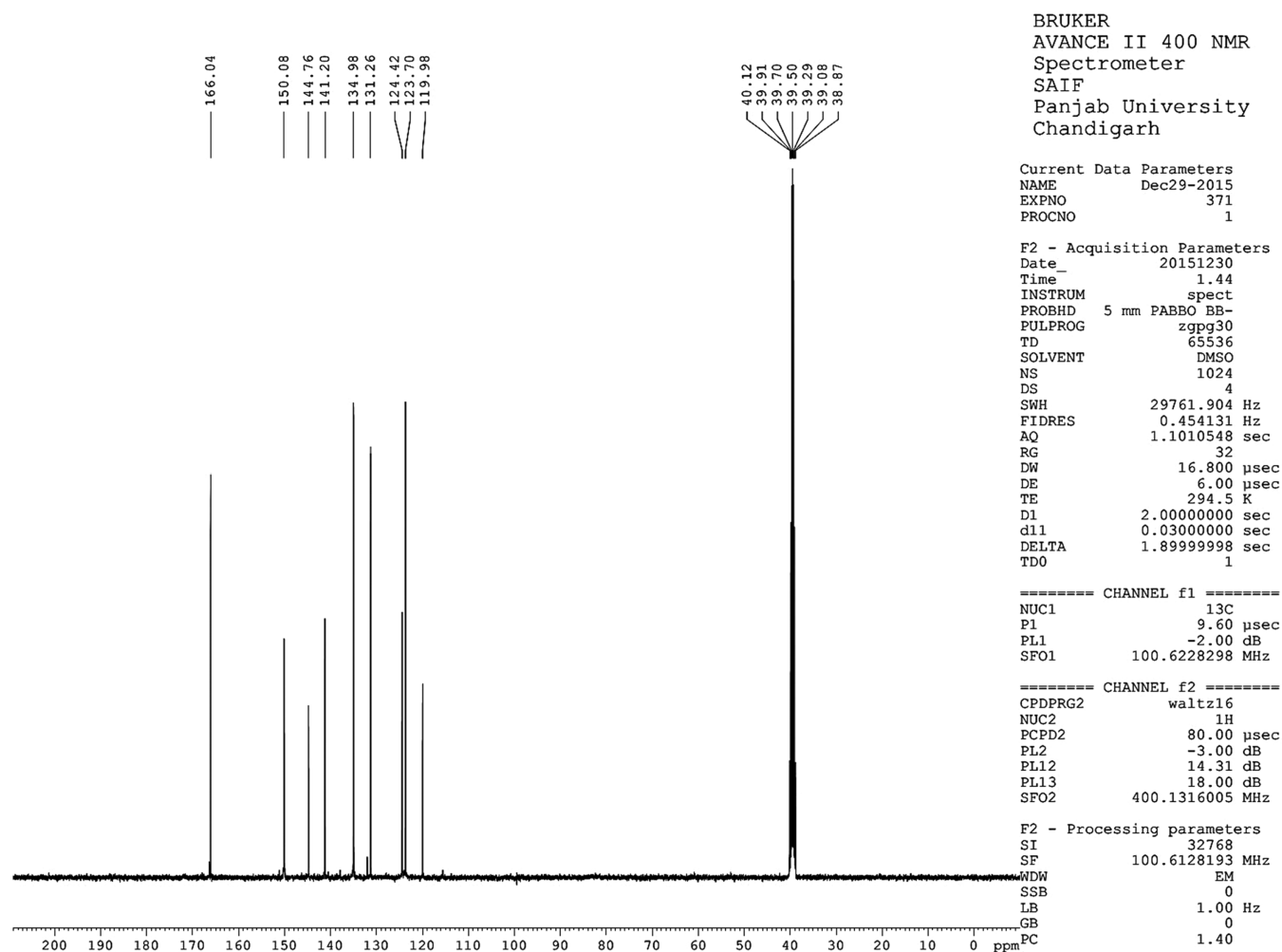


**Figure 6.** Linear regression between experimental and calculated chemical shifts ( $^{13}\text{C}$  NMR) for compound 14.

entry 2H7I) using the Schrodinger Glide module. It is one of the major enzymes engaged in the fatty acid biosynthesis type II pathway of *M. tuberculosis*.<sup>27</sup> The results of the *in vitro* study encouraged us to carry out molecular docking studies to

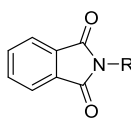
recognize the binding interaction of the synthesized compounds within the active site of InhA (Table 6). Docking validation has been first performed by redocking the co-crystallized structure into the active site of the InhA and measuring the root-mean-square deviation (RMSD) of the native co-crystallized ligand with redocked co-crystallized ligand, which was found to be 1.567 (Figure 9A). Overlay images of the docking validation are given in Figure 9A. Docking results demonstrated that synthesized compounds formed the crucial hydrogen-bond interaction with the isoindoline-1,3-dione *via* carbonyl oxygen. Compound 5 formed a hydrophobic  $\pi$ - $\pi$  interaction with Phe149, while compound 11 formed two hydrogen-bond interactions with Lys 165 and Tyr 158 (Figures 9B,C and 10A,B). The potent compound of the series (27) forms the hydrogen-bond interaction with the vital Tyr 158 residue *via* carbonyl oxygen, and the thiaziazol ring was involved in the hydrophobic  $\pi$ - $\pi$  interaction with Phe 147 and Tyr 158 (Figure 10C,D). Important residues within the 5 Å periphery of the ligands were Leu 218, Ile 215, Ile 194, Pro 193, Gly 192, Ala 191, Met 161, Tyr 158, Met 155, Phe 149, Asp 148, Met 147, and Met 103.

Based on the default parameters of the Prime MMGBSA modules implemented in Schrödinger, binding free energies ( $\Delta G$  bind) of protein–ligand complexes were calculated using the Glide pose viewer file. To determine the relative binding



**Figure 7.**  $^{13}\text{C}$  NMR spectrum of compound 14.

Table 5. Antimycobacterial and Cytotoxicity Study of the Synthesized Compounds (2–30)



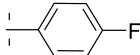
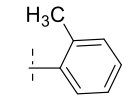
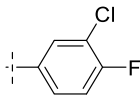
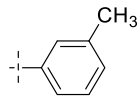
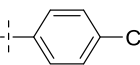
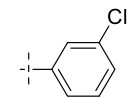
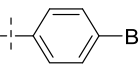
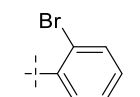
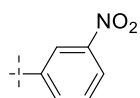
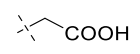
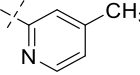
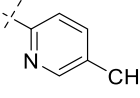
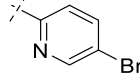
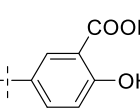
Compound Code	Structure	MIC (μM)	IC <sub>50</sub> (μM)	Cytotoxicity IC <sub>50</sub> (μM)	InhA IC <sub>50</sub> (μM)	LogP
2		> 200	197	---	---	2.816
3		194	68	---	---	2.492
4		186	64	---	---	3.627
5		100	29	> 150	---	2.892
6		94	28	> 150	---	3.386
7		96	26	> 150	---	3.386
8		102	31	> 150	---	3.536
9		> 200	75	---	---	3.076
10		> 200	121	---	---	2.736
11		164	55	---	---	0.881
12		> 200	160	---	---	2.295
13		> 200	148	---	---	2.295
14		> 200	90	---	---	2.782
15		> 200	92	---	---	2.534

Table 5. continued

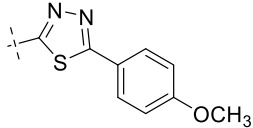
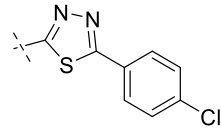
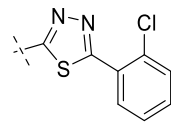
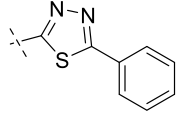
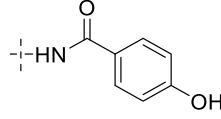
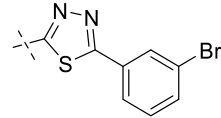
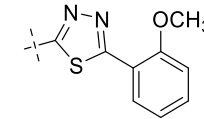
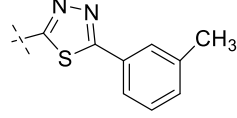
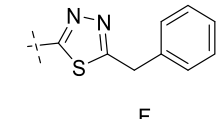
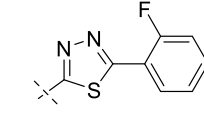
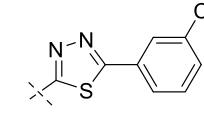
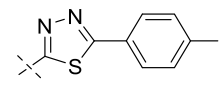
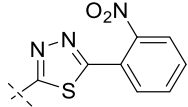
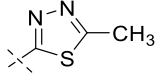
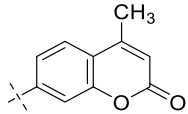
Compound Code	Structure	MIC ( $\mu\text{M}$ )	IC <sub>50</sub> ( $\mu\text{M}$ )	Cytotoxicity IC <sub>50</sub> ( $\mu\text{M}$ )	InhA IC <sub>50</sub> ( $\mu\text{M}$ )	LogP
16		182	62	---	---	3.028
17		> 200	> 200	---	---	3.686
18		> 200	91	---	---	3.436
19		> 200	> 200	---	---	2.969
20		> 200	101	---	---	0.389
21		> 200	100	---	---	3.836
22		180	58	---	---	2.468
23		123	43	---	---	3.468
24		> 200	> 200	---	---	2.938
25		> 200	133	---	---	3.116
26		192	80	---	---	3.686
27		64	18	> 200	8.65	4.096

Table 5. continued

Compound Code	Structure	MIC ( $\mu\text{M}$ )	IC <sub>50</sub> ( $\mu\text{M}$ )	Cytotoxicity IC <sub>50</sub> ( $\mu\text{M}$ )	InhA IC <sub>50</sub> ( $\mu\text{M}$ )	LogP
28		> 200	171	---	---	2.720
29		> 200	100	---	---	1.370
30		> 200	> 200	---	---	2.990
Std.	Isoniazid	0.38	0.15	---	---	-0.64
Std.	Triclosan	---	---	---	1.32	4.86

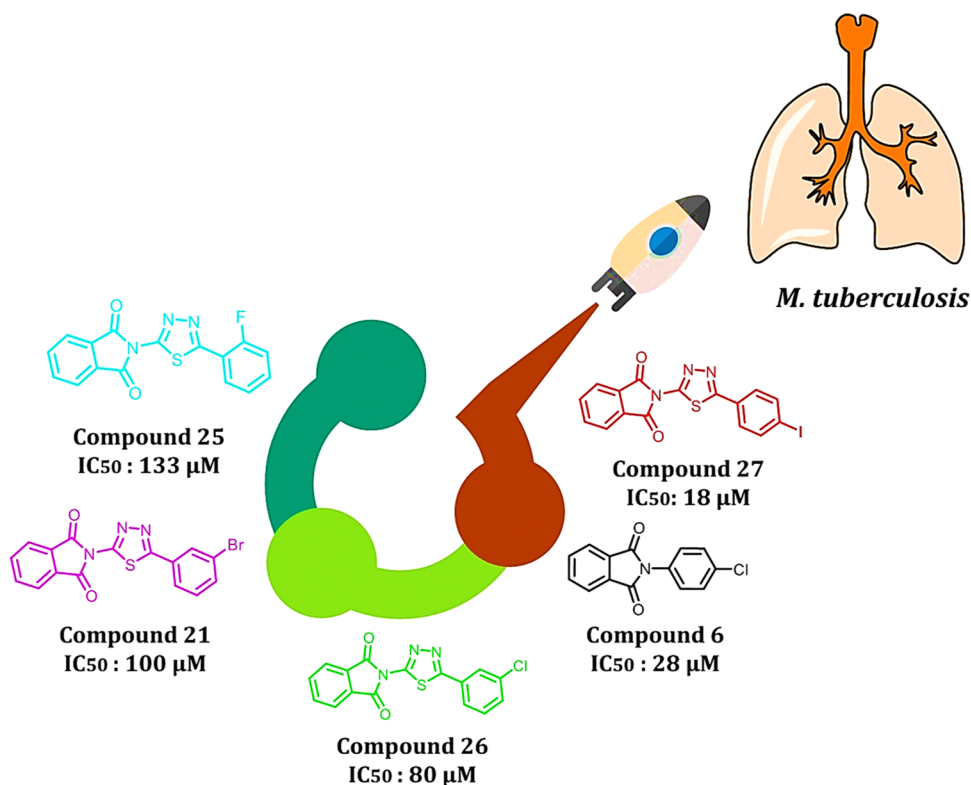


Figure 8. Structure–activity relationship of isoindoline-1,3-diones (2–30).

affinity of ligands to receptors, MMGBSA calculations are used; the lower the value, the stronger the binding affinity (Table 7).<sup>28</sup> Among the synthesized compounds, compound 18 ( $\Delta G_{\text{bind}} = -78.48$  kcal/mol), compound 25 ( $\Delta G_{\text{bind}} = -75.42$  kcal/mol), compound 26 ( $\Delta G_{\text{bind}} = -74.37$  kcal/mol), compound 21 ( $\Delta G_{\text{bind}} = -73.75$  kcal/mol), compound 28 ( $\Delta G_{\text{bind}} = -70.77$  kcal/mol), compound 30 ( $\Delta G_{\text{bind}} = -66.21$  kcal/mol), compound 17 ( $\Delta G_{\text{bind}} =$

$-65.71$  kcal/mol), and compound 27 ( $\Delta G_{\text{bind}} = -65.10$  kcal/mol) had significant affinity with the enzyme.

**2.7. DFT Reactivity.** Molecular boundary orbitals play a crucial role in a chemical reaction, and many chemical reactions occur by taking or giving electrons. An electron orbital with the highest energy is called a highest occupied molecular orbital (HOMO), while an electron orbital with the lowest energy is called a lowest unoccupied molecular orbital (LUMO). An electron that is being received by a molecule will



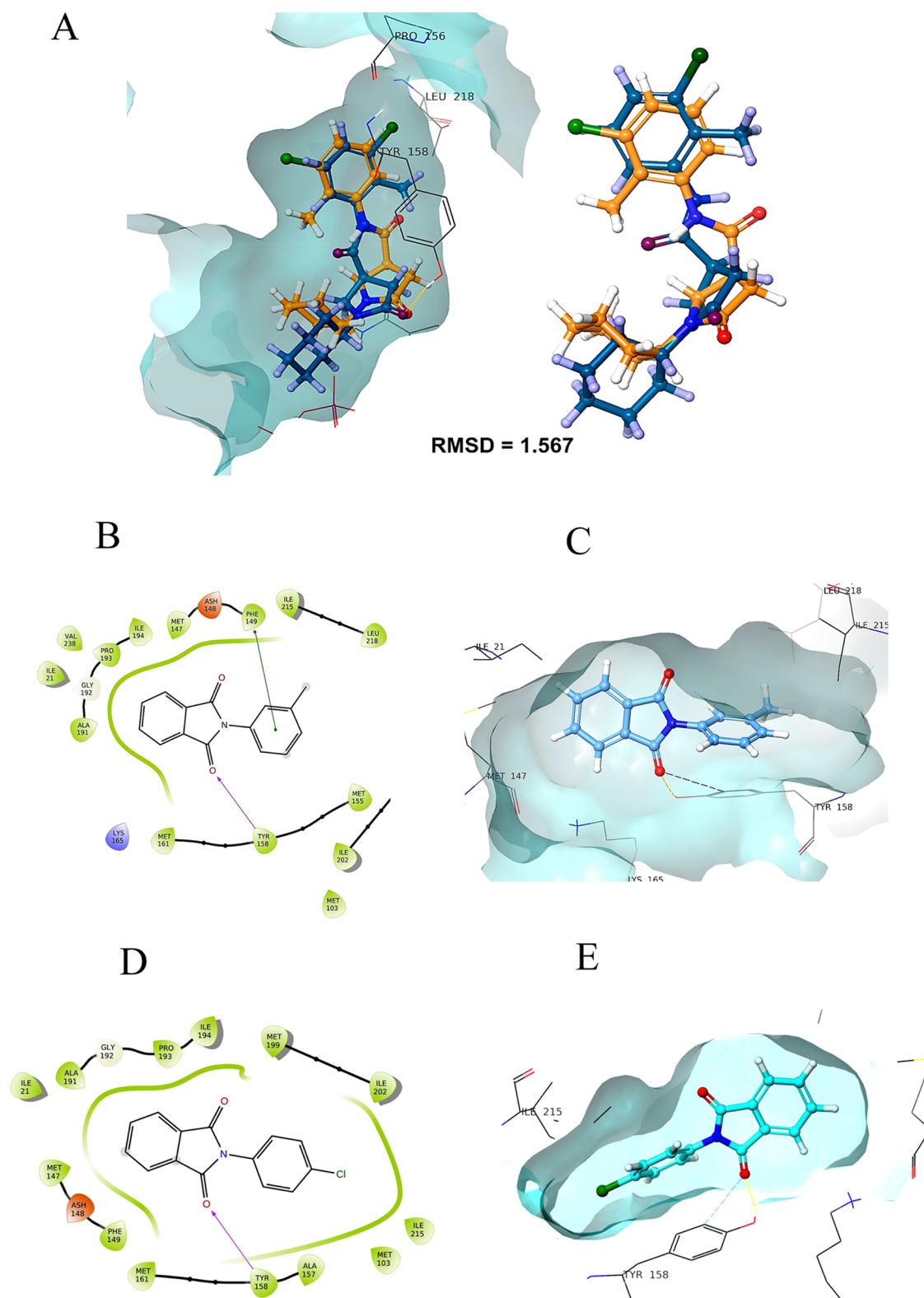


**Figure 9.** (A) Docking validation; (B, C) binding pose of compound 5 with InhA; (D, E) binding interaction of compound 6 with InhA.

chemical potential compared with other compounds in the series (Table 8).

The electrophilicity index measures a species' ability to accept electrons ( $\omega$ ).<sup>32–35</sup> Comparison of the IP values (electron-releasing tendency) of all synthesized compounds with electrophilic index (electron-accepting tendency) indicates that the IPs of all synthesized compounds are higher

than the electrophilic index and that compounds are more nucleophilic in nature (Table 8).

**2.10. Molecular Dynamic (MD) Simulation Study.** Since protein rigid crystal structure was used in molecular docking studies, molecular dynamic simulation was performed to explore the stability of the bound conformation of compound 27 within the binding cavity of InhA to investigate

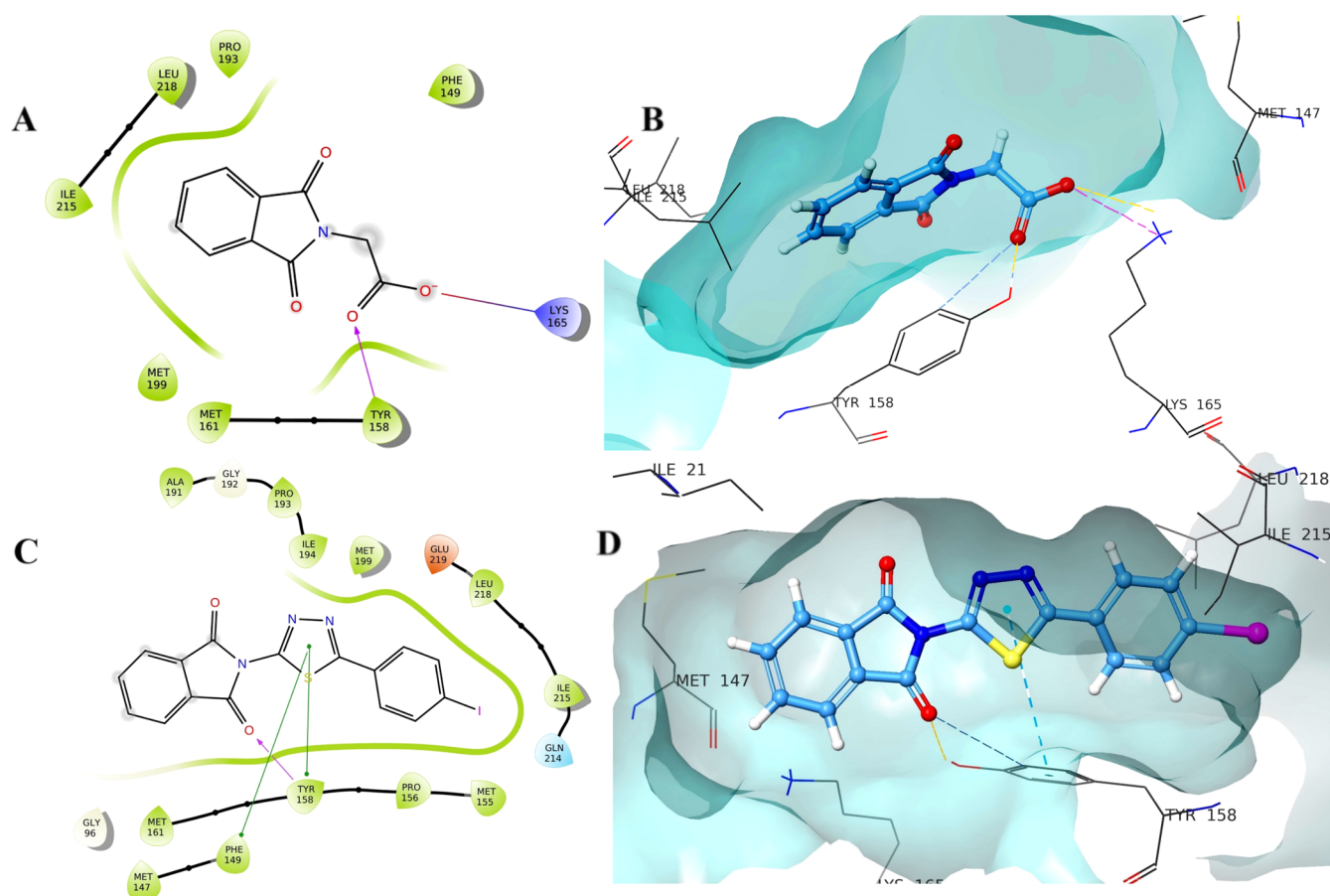


**Figure 10.** (A, B) Binding pose of compound 11 with InhA; (C, D) binding interaction of compound 27 with InhA.

ligand–protein complex interactions in the dynamic behavior. We simulated the systems up to 100 ns to explore the compound 27–InhA complex conformational stability and its changes. In this study, a 100 ns period was employed, which is enough time for the configurations of InhA  $C\alpha$  atoms in complex with compound 27.

The RMSD values of the protein backbone were used to calculate the stability of the protein–ligand complex throughout the dynamic simulation, as shown in Figure 12A. It is anticipated that the lower RMSD value during the simulation reveals that the protein–ligand complex is more stable. In contrast, the higher the RMSD value, the less stable is the protein–ligand complex.<sup>36</sup> The ligand RMSDs initially fluctuated between 20 and 30 ns due to the equilibration, after which the RMSD remained stable till the end of the simulation. It was observed that the protein had minor RMSD fluctuations during the 20–30 ns, followed by constant stability with an RMSD of 2.1 Å for the remaining time of simulation.

The “root-mean-square fluctuation (RMSF)” values for each amino acid residue in the protein backbone are illustrated in Figure 12B. In this graph, the peaks represent the fluctuation of each amino acid residue over the entire simulation. It implies that higher RMSF values represent higher residue flexibility, whereas lower RMSF values reflect less residue flexibility and better system stability. The  $\alpha$ -helical and  $\beta$ -strand areas (secondary structural components) are depicted in red and blue, and loop area is present in the white in the background of the RMSF plot. The  $\alpha$ -helical and  $\beta$ -strand are usually stiffer than the unstructured portion of the protein; hence, they fluctuate less than loop areas. A slight fluctuation of the

residues in the active site and main chain fluctuated indicated that the conformational change was minimal, implying that the reported lead compound was firmly bound within the cavity of the target protein binding pocket.<sup>37</sup> For 100 ns, the MD simulation of the compound 27–InhA complex was monitored and analyzed. As seen in Figure 12B, it is clear that there were no significant fluctuations in amino acid residues after the binding of compound 27 to the active site. The RMSF value of protein backbone residues in the catalytic domain is in the range of 0.5–3.5 Å. During the 100 ns time of simulation, compound 27 has contacted with the 15 amino acids of Ile 215, Leu 207, Ile 202, Met 199, Thr 196, Ile 194, Ala 191, Met 161, Tyr 158, Ala 157, Met 155, Phe 149, Met 147, Met 103, and Ile 21 (Figure 12B). Protein–ligand contact analysis shows that the residues Ile 194 exhibited 95% and Tyr 158 showed 22% hydrogen-bond interactions with the carbonyl oxygen of compound 27. Apart from this, Tyr 158 was also involved in the hydrophobic interaction with the 1,3,4-thiadiazole ring of compound 27 (Figure 12C,D).

We have also analyzed the ligand properties of the simulated compound 27, and its RMSD was observed to be below 1.2 Å. Radius of gyration (RG) is a measure of the extendness of the ligand; after 40 ns, RG was stable and found to be less than 4.40 Å. Ligand has not formed any kind of intramolecular hydrogen bonding with the receptor during the 100 ns simulation. Molecular surface area (MolSA) corresponds to the van der Waals surface area, and it was found to be 288–291 Å<sup>2</sup>, indicating the polar nature of the ligand. Solvent-accessible surface area (SASA) is the area of a molecule that is accessible to water molecules, and it was observed to be between 40 and

Table 7. Binding Free Energies of the Synthesized Compounds (2–30) by MMGBSA

compound code	MMGBSA $\Delta G$ bind	MMGBSA $\Delta G$ bind Coulomb	MMGBSA $\Delta G$ bind covalent	MMGBSA $\Delta G$ bind Hbond	MMGBSA $\Delta G$ bind Lipo	MMGBSA $\Delta G$ bind packing	MMGBSA $\Delta G$ bind solv GB	MMGBSA $\Delta G$ bind vdW
18	-78.48	-13.55	-1.99	-0.63	-30.35	-3.32	16.42	-45.07
25	-75.42	-13.55	-0.77	-0.62	-28.24	-3.27	16.34	-45.3
26	-74.37	-11.2	-0.71	-0.64	-29.34	-2.68	15.26	-45.06
21	-73.75	-11.36	-0.75	-0.64	-27.03	-2.67	14.78	-46.09
28	-70.77	-6.24	0.98	-0.63	-27.27	-3	11.65	-46.25
30	-66.21	-12.59	1.28	-0.85	-27.22	-3.58	19.34	-42.58
17	-65.71	-4.21	0.52	-0.54	-27.64	-4.69	11.14	-40.29
27	-65.10	-3.93	0.91	-0.51	-25.64	-4.71	11.57	-42.79
4	-64.72	-4.9	0.94	-0.86	-26.11	-3.86	12.55	-42.47
23	-64.45	-3.67	1.23	-0.09	-26.66	-2.99	15.27	-47.53
24	-63	-4.53	-0.15	-0.72	-27.66	-3.46	14.69	-41.18
4	-59.11	-7.02	4.38	-0.53	-22.85	-2.95	9.24	-39.37
10	-58.78	-3.63	2.04	-0.67	-23.15	-3.06	10.54	-40.83
6	-57.92	-6.77	3.65	-0.56	-22.39	-2.63	9.98	-39.21
5	-57.1	-8.39	3.4	-0.56	-23.1	-2.49	13.31	-39.25
7	-56.53	-6.14	1.83	0	-24.53	-3.06	13.6	-38.24
15	-56.03	3.09	1.28	-1.02	-23.04	-3.07	8.91	-42.18
13	-55.86	-11.42	2.54	-0.56	-20.69	-2.45	14.22	-37.5
9	-55.55	-12.67	0.84	-0.56	-20.51	-2.63	14.47	-34.48
3	-53.02	-8.63	0.51	-0.52	-21.74	-1.82	14.08	-34.9
29	-52.32	-3.99	-0.24	-0.1	-19.59	-2.97	11.27	-36.69
8	-51.96	-2.48	2.07	0	-23.39	-3.04	14.21	-39.34
20	-51.9	-5.62	4.03	-0.98	-22.19	-2.39	19.7	-44.46
14	-51.55	-3.33	0.79	-0.05	-21.48	-2.94	14.95	-39.49
2	-50.73	-9.72	-0.71	0	-21.6	-2.19	13.4	-29.91
12	-50.36	-5.54	-0.96	0	-21.56	-2.21	12.39	-32.49
20	-35.46	-7.72	3.65	-0.98	-21.93	-2.33	39.39	-45.54
11	-35.18	-0.9	0.91	-0.79	-13.81	-2.57	9.13	-27.15
20	-29.33	-37.99	9.63	-0.55	-15.9	-2.02	64.12	-46.62

50 Å<sup>2</sup>. The polar surface area (PSA) of a molecule is the solvent-accessible surface area contributed only by oxygen and nitrogen. It was found to be 114–120 Å<sup>2</sup> due to the enrichment of the compound 27 with oxygen and nitrogen (Figure 12E). We have also calculated the per residue binding free energy when the ligand–receptor complex was stable during the simulation (at 99 ns frame), and Asp-261 (−70.85), Asp 89 (−70.85), Asn 187 (−70.85), Gln 30 (−70.85), Gln 32 (−70.85), Asp 115 (−70.85), Asn 172 (−70.85), Asp 18 (−70.85), Asp 234 (−70.85), Asp 256 (−70.85), Asp 223 (−70.85), and Gln 214 (−70.85) had the lowest per residue energy, indicating their active involvement in the interaction with compound 27 (Figure 13).

InhA macrodomain protein after binding with compound 27 is studied through the dynamic cross-correlation matrix (DCCM) analysis to determine the correlated mobility of structural domains. All pairwise correlation coefficient calculations were performed to calculate the DCCM. In the graphical representation, correlation values range from −1 to +1, and the colors reflect the intensity of the motion between residues, ranging from red to blue. Blue colors indicate a positive (+1/complete) correlation, white colors indicate no correlation, and red colors indicate a negative (−1/complete anti) correlation. Using the correlation scores on the central mean line (blue), we identified three separate blocks where amino acid movement was highly correlated.<sup>38</sup>

Domain D1 (InhA) has the highest cross-correlation of residues composed of 50–100 residues embedded into one helix, distinct  $\beta$ -sheets, and an extended loop (red), while

domain D2 (InhA) contains 140–190 residues rooted in one helix, distinct  $\beta$ -sheets, and an extended loop (pink). The D3 domain extends from 220 to 250 residues, spanning the three helices and one extended loop (green). These residues in D1, D2, and D3 domains are highly correlated and are in good agreement with the RMSF of the C- $\alpha$  backbone of macrodomain proteins in the compound 27-bound state, with moderate to fewer fluctuations of respective amino acid residues (Figure 14). The trajectory-derived MD simulations were also analyzed with principal component analysis (PCA) to study the conformational distribution during simulation time and the large-scale collective motions of the protein interacting with ligands.<sup>38</sup> In all of the complexes, phase space projection of protein motion along PC1 and PC2 revealed a uniform distribution of conformations through the simulations (Figure 15).

To perform the postdynamic MMGBSA analysis, the 10 frames of the MD simulation of compound 27 were produced at intervals of 10 ns each. Compound 27 shows a postdynamic binding free energy of −78.96 kcal/mol ( $\Delta G$  bind average of 10 frames) (Table 9).

### 3. CONCLUSIONS

In conclusion, isoindoline-1,3-dione derivatives (2–30) were synthesized and evaluated for their antimycobacterial activity against the H<sub>37</sub>Rv strain. Among the synthesized compounds, compound 27 was the most potent compound of the series, with an IC<sub>50</sub> value of 18  $\mu$ M. The InhA inhibitory (IC<sub>50</sub>) activity of compound 27 was 8.65  $\mu$ M in comparison to



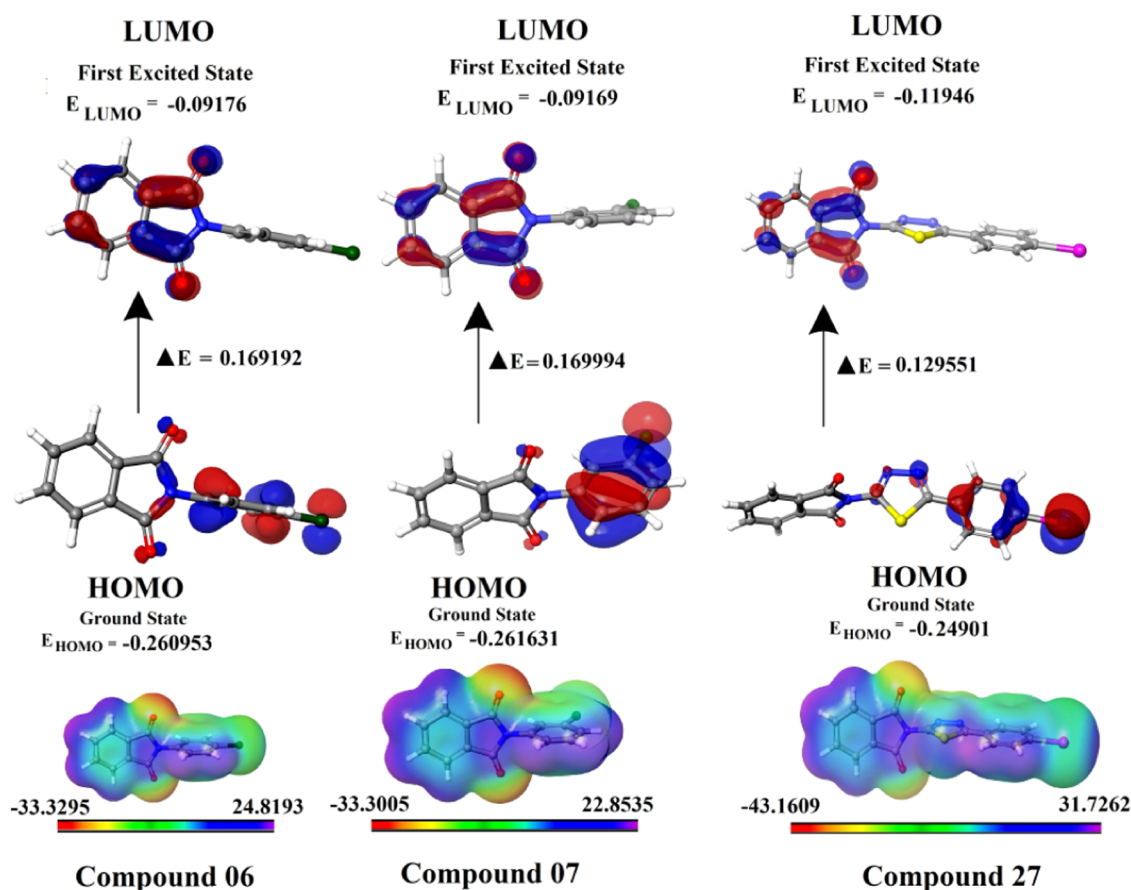


Figure 11. DFT-based frontier molecular orbital energies calculations of HOMO, LUMO, and maximum electrostatic potential (MESP).

Triclosan ( $1.32 \mu\text{M}$ ). We used the DFT/B3LYP method to correlate experimental IR,  $^1\text{H}$  NMR, and  $^{13}\text{C}$  NMR spectral data with theoretical quantum-mechanics-based computational ones, and a significant co-relationship was observed. SAR study suggests that 1,3,4-thiadiazols are more potent than the substituted anilines at the second position of the 2-isoindoline-1,3-dione. Iodophenyl was more potent than chloro-, bromo-, and fluorophenyl among the halo-phenyl-substituted 1,3,4-thiadiazols at the second position. A docking study demonstrated that synthesized compounds formed the crucial hydrogen-bond interaction with the Tyr 158 residue of the InhA enzyme.

The DFT study of the synthesized compounds explained the reactivity of the compounds, and compounds 15, 11, 27, 23, 17, 24, 19, and 21 had less energy gap, which indicates their high reactivity and electron transfer capacity. The MESP calculation has elaborated on the electrophilic and nucleophilic sites available on the compounds. An orange color has been observed around the carbonyl oxygens of the isoindoline-1,3-dione ring, indicating their nucleophilic nature. The docking study also reciprocated these results, where these carbonyl oxygens acted as a hydrogen-bond acceptor, forming a crucial hydrogen bond with the Tyr 158 residue. An MD simulation study of the compound 27–InhA complex indicated that the ligand remained stable in the InhA pocket for 100 ns. The stability of the compound 27–InhA complex was further validated by postdynamic MMGBSA, DCCM, and PCA, which validated the stability of the compound 27–InhA complex.

#### 4. EXPERIMENTAL SECTION

Unless otherwise specified, all reagents used in the studies were of commercial analytical quality (Sigma-Aldrich and Spectrochem Pvt. Ltd.). All reactions' progress was monitored through precoated silica gel GF254 thin-layer chromatography, and spots were visualized under UV light at 254 or 365 nm. Different solvent systems, hexane/ethyl acetate (6:4 and 7:3), toluene/ethyl acetate/formic acid (5:4:1 v/v/v) benzene/acetone (7:3 and 9:1 v/v), and chloroform/methanol (9:1 v/v), were used to run chromatography. The melting points of the synthesized compounds were determined using one-end open capillary tubes on an Analab Scientific Instruments melting-point apparatus. The NMR spectra were recorded in dimethyl sulfoxide ( $\text{DMSO}-d_6$ ) at Chandigarh Punjab University using a Bruker Avance-II 400 NMR spectrometer running at 400 MHz with TMS as an internal standard. Chemical shifts are presented in ppm units relative to TMS. *Cl<sub>o</sub>P* values were calculated using CHEMDRAW ultra 8.0 software.

**4.1. General Procedure for the Synthesis of Isoindoline-1,3-dione Derivatives.** Phthalic anhydride (0.1 mol) and the primary amino-containing compounds (0.1 mol) were mixed with 50–75 mL of glacial acetic acid. The mixture was refluxed for 3 h and diluted with water to obtain the title compounds. It is further recrystallized with ethanol, followed by column chromatography to get the pure product.

**4.1.1. 2-(4-Fluorophenyl)isoindoline-1,3-dione (2).** Yield: 64%, mp: 132–136 °C; IR  $\nu_{\text{max}}$  (KBr pellets): 3058.14 (CH stretch), 1762.52 (C=O cyclic amide), 1219.05 (C–F)  $\text{cm}^{-1}$ ;  $^1\text{H}$  NMR (400 MHz,  $\text{DMSO}-d_6$ ):  $\delta$  7.40–8.10 (m, 8H, Ar–

Table 8. DFT-Based Frontier Molecular Orbital (FMO) Energy Calculations of the Synthesized Compounds (2–30)

cmpd code	$E_{\text{HOMO}}$ (eV)	$E_{\text{LUMO}}$ (eV)	energy gap/ $\Delta E$ (eV) <sup>a</sup>	IP (eV) <sup>b</sup>	EA (eV) <sup>c</sup>	$\chi$ (eV) <sup>d</sup>	$\eta$ (eV) <sup>e</sup>	$s$ (eV <sup>-1</sup> ) <sup>f</sup>	$\mu$ (eV) <sup>g</sup>	$\omega$ (eV) <sup>h</sup>	MESP (kcal/mol)
2	-0.261021	-0.090118	0.170903	0.261021	0.090118	0.1755695	0.0854515	5.851272359	-0.1755695	0.180363419	-34.07 to 24.26
4	-0.264468	-0.094366	0.170102	0.264468	0.094366	0.179417	0.085051	5.878825646	-0.179417	0.189242101	-31.72 to 25.6
5	-0.253268	-0.085429	0.167839	0.253268	0.085429	0.1693485	0.0839195	5.958090789	-0.1693485	0.170871576	-37.05 to 22.7
6	-0.260953	-0.091761	0.169192	0.260953	0.091761	0.176357	0.084596	5.910444938	-0.176357	0.183825426	-33.31 to 24.71
7	-0.261631	-0.091693	0.169938	0.261631	0.091693	0.176662	0.084969	5.884499053	-0.176662	0.183652051	-33.58 to 24.63
8	-0.250107	-0.084632	0.165475	0.250107	0.084632	0.1673695	0.0827375	6.043208944	-0.1673695	0.16928569	-32.94 to 23.09
9	-0.249172	-0.080643	0.168529	0.249172	0.080643	0.1649075	0.0842645	5.933696871	-0.1649075	0.161363822	-34.9 to 21.54
10	-0.28238	-0.100517	0.181863	0.28238	0.100517	0.1914485	0.0909315	5.498644584	-0.1914485	0.201539225	-31.71 to 26.35
17	-0.251739	-0.100182	0.151557	0.251739	0.100182	0.1759605	0.0757785	6.598177583	-0.1759605	0.204293418	-35.11 to 26.97
18	-0.254641	-0.098278	0.156363	0.254641	0.098278	0.1764595	0.0781815	6.395374865	-0.1764595	0.199138896	-39.44 to 26.19
19	-0.250157	-0.097385	0.152772	0.250157	0.097385	0.173771	0.076386	6.545702092	-0.173771	0.19765638	-37.38 to 26.06
20	-0.243777	-0.087886	0.155891	0.243777	0.087886	0.1658315	0.0779455	6.414738503	-0.1658315	0.176405863	-39.59 to 59.53
21	-0.247944	-0.092945	0.154999	0.247944	0.092945	0.1704445	0.0774995	6.451654527	-0.1704445	0.187429129	-34.83 to 25.14
23	-0.245593	-0.096538	0.149055	0.245593	0.096538	0.1710655	0.0745275	6.708932944	-0.1710655	0.196326224	-38.1 to 25.71
24	-0.251974	-0.099263	0.152711	0.251974	0.099263	0.1756185	0.0763555	6.548316755	-0.1756185	0.201962253	-45.97 to 26.72
26	-0.258257	-0.100378	0.157879	0.258257	0.100378	0.1793175	0.0789395	6.333964618	-0.1793175	0.203667149	-35.39 to 27.01
27	-0.24901	-0.119459	0.129551	0.24901	0.119459	0.1842345	0.0647755	7.71896782	-0.1842345	0.261999915	-43.36 to 31.93
28	-0.265849	-0.101121	0.164728	0.265849	0.101121	0.183485	0.082364	6.070613375	-0.183485	0.204377794	-39.21 to 28.86
29	-0.27268	-0.097511	0.175169	0.27268	0.097511	0.1850955	0.0875845	5.708772671	-0.1850955	0.195584516	-37.91 to 26
30	-0.248783	-0.09323	0.155553	0.248783	0.09323	0.1710065	0.0777765	6.428677043	-0.1710065	0.187995237	-41.41 to 26.31
11	-0.049525	0.033402	0.082927	0.049525	-0.033402	0.0080615	0.0414635	12.0587987	-0.0080615	0.000783675	-141.85 to 26.2
12	-0.267635	-0.084162	0.183473	0.267635	0.084162	0.1758985	0.0917365	5.450393246	-0.1758985	0.168636706	-36.44 to 22.05
13	-0.263345	-0.083954	0.179391	0.263345	0.083954	0.1736495	0.0896955	5.574415662	-0.1736495	0.16809176	-36.35 to 22.08
14	-0.260984	-0.083605	0.177379	0.260984	0.083605	0.1722945	0.0886895	5.637645945	-0.1722945	0.167355745	-32.49 to 23.62
15	-0.042044	-0.00149	0.040554	0.042044	0.00149	0.021767	0.020277	24.65848005	-0.021767	0.011683244	-145.89 to 13.7

<sup>a</sup>Energy gap/ $\Delta E = E_{\text{HOMO}} - E_{\text{LUMO}}$ . <sup>b</sup>Ionization potential (IP) =  $-E_{\text{HOMO}}$ . <sup>c</sup>Electron affinity (EA) =  $-E_{\text{LUMO}}$ . <sup>d</sup>Electronegativity ( $\chi$ ) = (IP + EA)/2. <sup>e</sup>Chemical hardness ( $\eta$ ) = (IP - EA)/2. <sup>f</sup>Chemical softness ( $s$ ) =  $1/2\eta$ . <sup>g</sup>Chemical potential ( $\mu$ ) =  $-(\text{IP} + \text{EA})/2$ . <sup>h</sup>Electrophilic index ( $\omega$ ) =  $\mu^2/2\eta$ .

CH) ppm; <sup>13</sup>C NMR (DMSO-*d*<sub>6</sub>)  $\delta$  167.45, 162.53, 133.34, 132.35, 130.53, 128.46, 123.23, 114.24 ppm; LCMS: purity: 100%; RT: 6.106 (254  $\lambda$ );  $m/z$ : 241.00 [ $M^+$ ].

4.1.2. 2-(*o*-Tolyl)isoindoline-1,3-dione (**3**). Yield: 74%, mp: 166–172 °C. IR  $\nu_{\text{max}}$  (KBr pellets): 3021.14 (Aro. CH stretch), 2881.34 (Ali. CH stretch), 1756.11 (C=O cyclic amide)  $\text{cm}^{-1}$ ; <sup>1</sup>H NMR (400 MHz, DMSO-*d*<sub>6</sub>):  $\delta$  7.10–8.12 (m, 8H, Ar-CH), 2.42 (s, 3H, CH<sub>3</sub>) ppm; <sup>13</sup>C NMR (DMSO-*d*<sub>6</sub>) 165.24, 136.54, 134.54, 132.42, 131.35, 130.46, 130.10, 129.53, 125.93, 122.83, 18.42 ppm; LCMS: purity: 100%; RT: 5.991 (254  $\lambda$ );  $m/z$ : 237.9 [ $M^+$ ].

4.1.3. 2-(3-Chloro-4-fluorophenyl)isoindoline-1,3-dione (**4**). Yield: 71%, mp: 182–188 °C. IR  $\nu_{\text{max}}$  (KBr pellets):

3033.16 (CH stretch), 1753 (C=O cyclic amide), 1053.17 (C-F), 596.02 (C-Cl)  $\text{cm}^{-1}$ ; <sup>1</sup>H NMR (400 MHz, DMSO-*d*<sub>6</sub>): 7.20–8.12 (m, 7H, Ar-CH) ppm; <sup>13</sup>C NMR (DMSO-*d*<sub>6</sub>)  $\delta$  168.23, 154.44, 136.34, 134.35, 130.17, 129.42, 126.45, 123.56, 120.93, 112.56 ppm; LCMS: purity: 100%; RT: 6.424 (254  $\lambda$ );  $m/z$ : 275.1 [ $M^+$ ] and 277.5 [ $M + 2$ ].

4.1.4. 2-(*m*-Tolyl)isoindoline-1,3-dione (**5**). Yield: 66%, mp: 168–172 °C. IR  $\nu_{\text{max}}$  (KBr pellets): 3058.09 (Aro. CH stretch), 2845.23 (Ali. CH stretch), 1740.04 (C=O cyclic amide)  $\text{cm}^{-1}$ ; <sup>1</sup>H NMR (400 MHz, DMSO-*d*<sub>6</sub>): 6.95–7.83 (m, 8H, Ar-CH), 2.41 (s, 3H, CH<sub>3</sub>) ppm; <sup>13</sup>C NMR (DMSO-*d*<sub>6</sub>)  $\delta$  165.20, 138.36, 131.73, 132.56, 130.85, 129.25, 128.85,

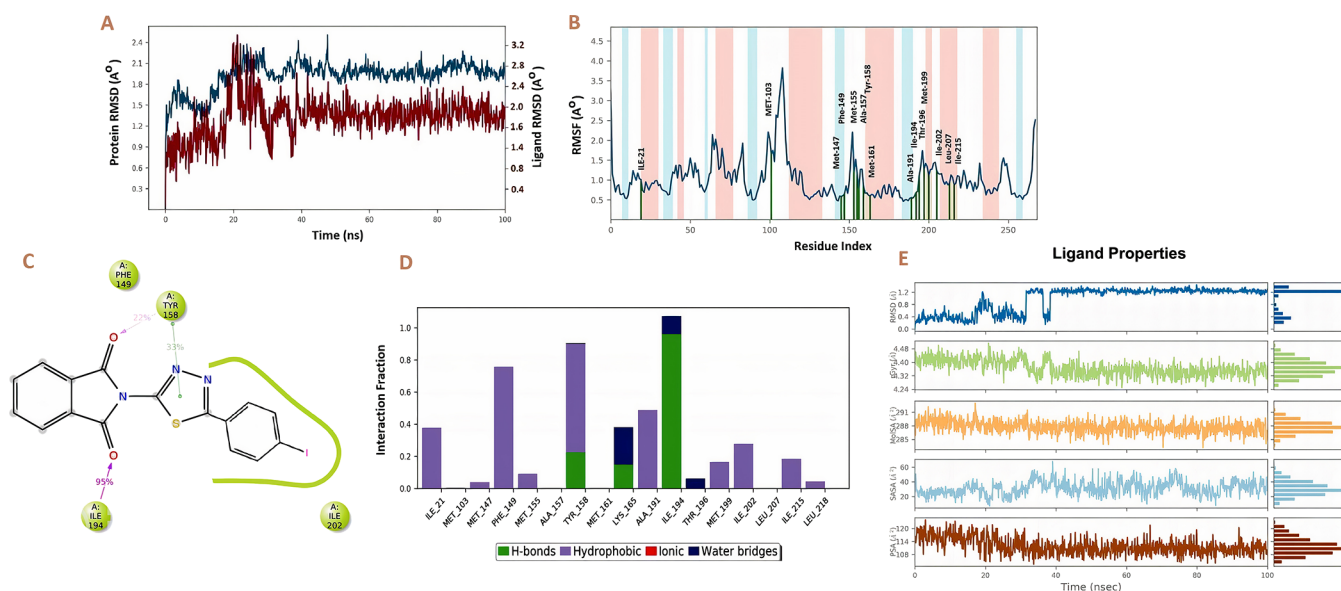


**Figure 12.** (A) Protein (InhA) and ligand (compound 27) RMSD; (B) root-mean-square fluctuation (RMSF) of the InhA; (C) different interactions of compound 27 during 100 ns with InhA; (D) interaction fraction of different residues with compound 27 during 100 ns; and (E) ligand (compound 27) properties.

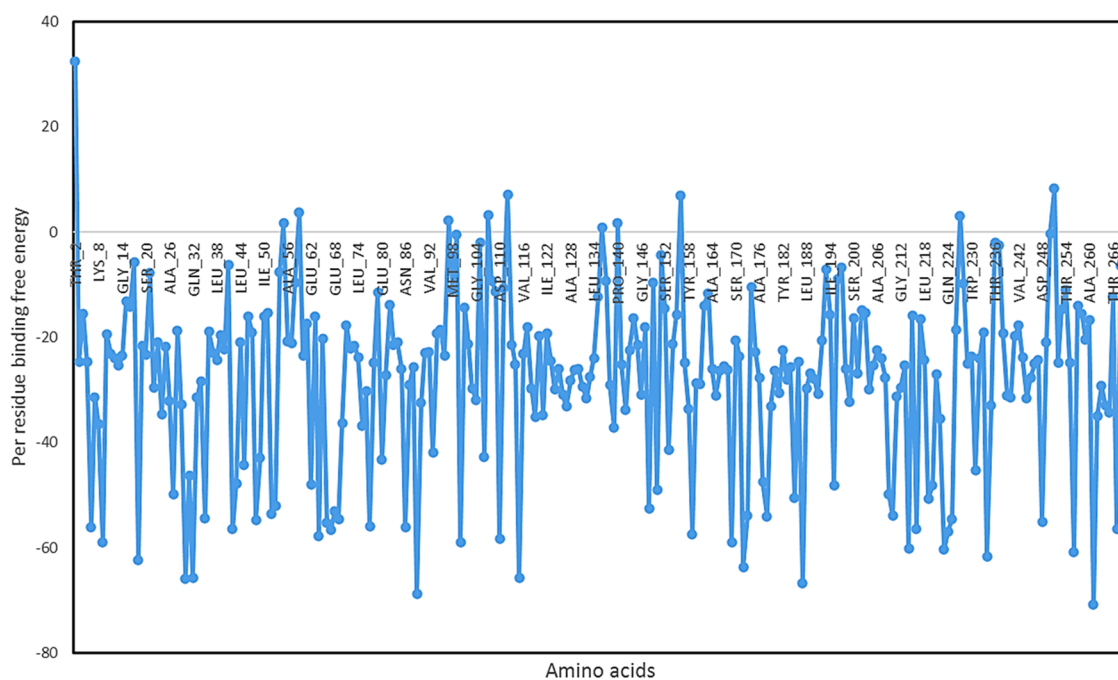


**Figure 13.** Per residue binding free energy of the InhA with compound 27.

125.14, 124.65, 122.68, 20.43 ppm; LCMS: purity: 100%; RT: 6.154 (254  $\lambda$ );  $m/z$ : 237.8 [ $M^+$ ].

**4.1.5. 2-(4-Chlorophenyl)isoindoline-1,3-dione (6).** Yield: 66%, mp: 190–194 °C. IR  $\nu_{\max}$  (KBr pellets): 3050.08 (Aro. CH stretch), 1745.05 (C=O cyclic amide), 749.08 (C–Cl)  $\text{cm}^{-1}$ ;  $^1\text{H}$  NMR (400 MHz, DMSO- $d_6$ ): 7.45–8.14 (m, 8H, Ar–CH);  $^{13}\text{C}$  NMR (DMSO- $d_6$ )  $\delta$  167.45, 137.45, 136.67, 135.34, 130.99, 130.12, 129.60, 125.67 ppm; LCMS: purity: 100%; RT: 6.349 (254  $\lambda$ );  $m/z$ : 257.8 [ $M^+$ ] and 259.7 [ $M + 2$ ].

**4.1.6. 2-(3-Chlorophenyl)isoindoline-1,3-dione (7).** Yield: 62%, mp: 176–182 °C. Yield: 66%, mp: 190–194 °C. IR  $\nu_{\max}$  (KBr pellets): 3042.23 (CH stretch), 1749.11 (C=O cyclic

amide), 785.88 (C–Cl)  $\text{cm}^{-1}$ ;  $^1\text{H}$  NMR (400 MHz, DMSO- $d_6$ ): 7.120–8.21 (m, 8H, Ar–CH);  $^{13}\text{C}$  NMR (DMSO- $d_6$ )  $\delta$  167.53, 134.5, 133.76, 134.1, 133.2, 132.45, 130.3, 127.9, 126.2, 124.23 ppm; purity: 100%; RT: 6.351 (254  $\lambda$ );  $m/z$ : 257.9 [ $M^+$ ] and 259.2 [ $M + 2$ ].

**4.1.7. 2-(4-Bromophenyl)isoindoline-1,3-dione (8).** Yield: 64%, mp: 252–254 °C. IR  $\nu_{\max}$  (KBr pellets): 3142.06 (CH stretch), 1739.97 (C=O cyclic amide), 650.04 (C–Br)  $\text{cm}^{-1}$ ;  $^1\text{H}$  NMR (400 MHz, DMSO- $d_6$ ): 7.12–8.18 (m, 8H, Ar–CH);  $^{13}\text{C}$  NMR (DMSO- $d_6$ )  $\delta$  168.87, 138.45, 136.24, 132.77, 130.12, 128.23, 126.73, 122.34 ppm; LCMS: purity: 100%; RT: 6.459 (254  $\lambda$ );  $m/z$ : 302.4 [ $M^+$ ] and 304.9 [ $M + 2$ ].

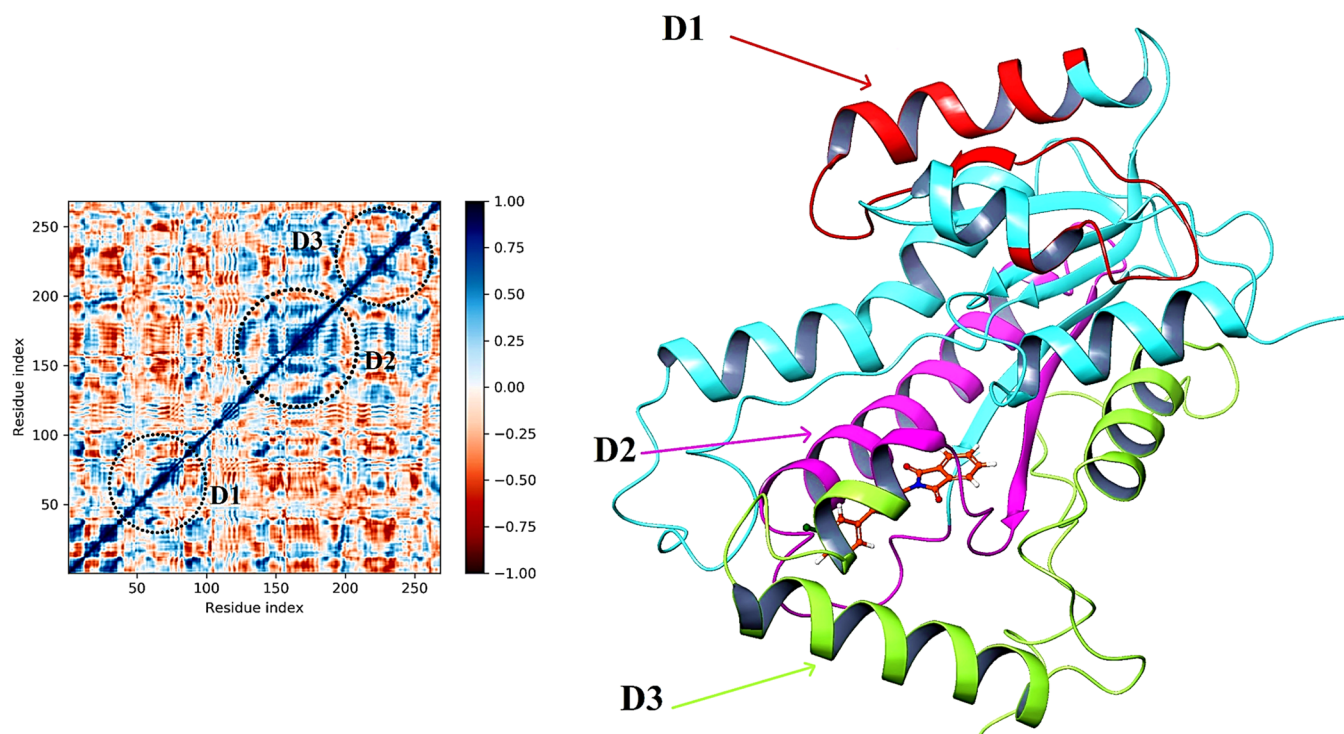


Figure 14. DCCM analysis of compound 27 (D1, D2, and D3 are highly correlated residues of the InhA).

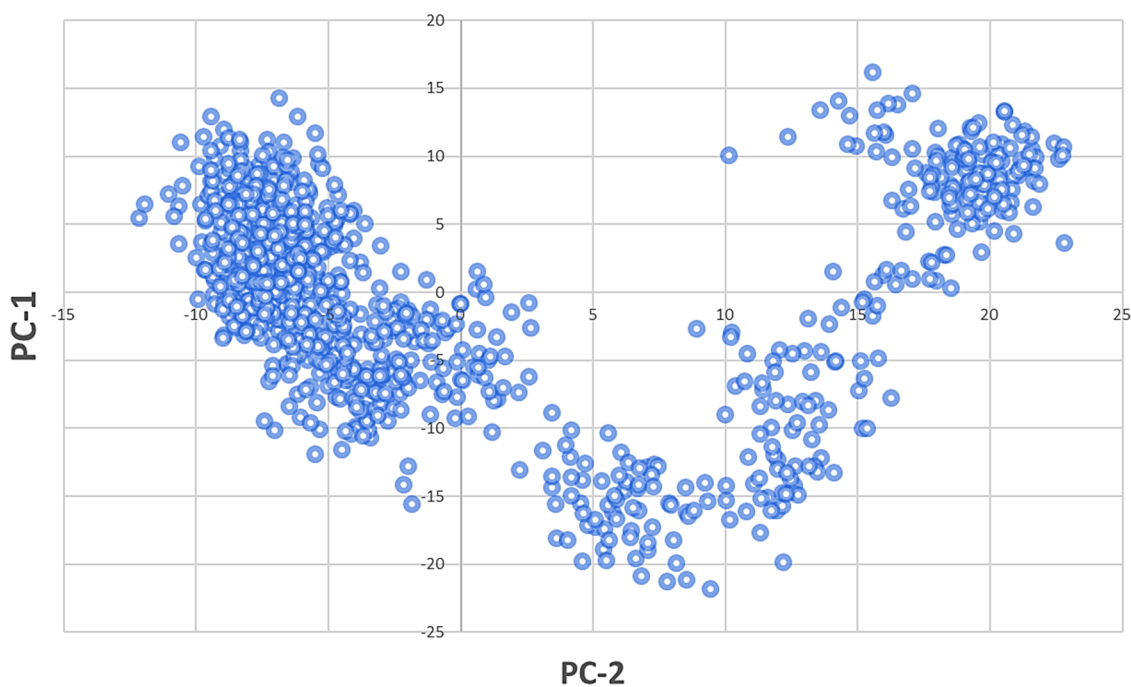


Figure 15. PCA of compound 27.

4.1.8. 2-(2-Bromophenyl)isoindoline-1,3-dione (**9**). Yield: 67%, mp: 242–250 °C. IR  $\nu_{\max}$  (KBr pellets): 3123.24 (CH stretch), 1723.34 (C=O cyclic amide), 665.04 (C–Br)  $\text{cm}^{-1}$ ;  $^1\text{H}$  NMR (400 MHz, DMSO- $d_6$ ): 7.15–8.21 (m, 8H, Ar–CH);  $^{13}\text{C}$  NMR (DMSO- $d_6$ )  $\delta$  169.34, 142.55, 137.45, 134.24, 132.88, 131.38, 123.38, 125.73, 122.66 ppm; LCMS: purity: 100%; RT: 5.936 (254  $\lambda$ );  $m/z$ : 302.9 [ $\text{M}^+$ ] and 304.6 [ $\text{M} + 2$ ].

4.1.9. 2-(3-Nitrophenyl)isoindoline-1,3-dione (**10**). Yield: 70%, mp: 278–284 °C. IR  $\nu_{\max}$  (KBr pellets): 3058 (CH

stretch), 1699 (C=O cyclic amide)  $\text{cm}^{-1}$ ;  $^1\text{H}$  NMR (400 MHz, DMSO- $d_6$ ): 6.85–8.48 (m, 8H, Ar–CH);  $^{13}\text{C}$  NMR (DMSO- $d_6$ )  $\delta$  168.65, 148.15, 134.34, 134.22, 133.56, 132.24, 130.23, 123.73, 121.54, 118.75 ppm; LCMS: purity: 100%; RT: 5.960 (254  $\lambda$ );  $m/z$ : 268.1 [ $\text{M}^+$ ].

4.1.10. 2-(1,3-Dioxoisoindolin-2-yl)acetic Acid (**11**). Yield: 66%, mp: 204–206 °C. IR  $\nu_{\max}$  (KBr pellets): IR  $\nu_{\max}$  (KBr pellets): 3598.91 (OH stretch), 3123.59 (CH stretch), 1726.00 (C=O cyclic amide)  $\text{cm}^{-1}$ ;  $^1\text{H}$  NMR (400 MHz, DMSO- $d_6$ ): 12.12 (s, 1H, COOH), 7.24–7.99 (m, 4H, Ar–

Table 9. Postsimulation Binding Free Energy Calculation of Compound 27

complex detail	MMGBSA $\Delta G$ bind	MMGBSA $\Delta G$ bind Coulomb	MMGBSA $\Delta G$ bind Hbond	MMGBSA $\Delta G$ bind Lipo	MMGBSA $\Delta G$ bind packing	MMGBSA $\Delta G$ bind vdW
at 10 ns	-87.78	-17.009	-0.974	-29.699	-4.086	-52.885
at 20 ns	-85.41	-18.424	-1.015	-27.228	-2.497	-53.606
at 30 ns	-77.70	-10.923	-0.685	-28.180	-4.794	-51.507
at 40 ns	-82.74	-12.108	-0.692	-28.834	-4.796	-50.101
at 50 ns	-69.77	-9.402	-0.465	-25.391	-4.264	-45.616
at 60 ns	-74.29	-6.559	-0.463	-26.718	-4.0120	-48.644
at 70 ns	-73.11	-12.185	-0.597	-25.710	-4.781	-45.266
at 80 ns	-77.25	-10.276	-0.640	-25.762	-3.735	-49.196
at 90 ns	-81.46	-9.165	-0.515	-27.805	-3.642	-52.073
at 100 ns	-80.123	-10.553	-0.578	-26.822	-4.312	-50.787
average	-78.9690	-11.660	-0.662	-27.215	-4.092	-49.968

H), 4.32 (s, 1H, Ali-CH<sub>2</sub>) ppm; <sup>13</sup>C NMR (DMSO-*d*<sub>6</sub>) 170.32, 169.34, 138.76, 132.35, 126.42, 40.45 ppm; LCMS: purity: 100%; RT: 3.379 (254  $\lambda$ ); *m/z*: 205.1 [M<sup>+</sup>].

4.1.11. 2-(4-Methylpyridin-2-yl)isoindoline-1,3-dione (**12**). Yield: 64%, mp: 172–184 °C. IR  $\nu_{\max}$  (KBr pellets): 3051.13 (Aro. CH stretch), 2951.19 (Ali. CH stretch), 1755.95 (C=O) cm<sup>-1</sup>; <sup>1</sup>H NMR (400 MHz, DMSO-*d*<sub>6</sub>): 7.34–8.16 (s, 7H, Ar-H), 2.31 (s, 3H, CH<sub>3</sub>) ppm; <sup>13</sup>C NMR (DMSO-*d*<sub>6</sub>) 164.34, 151.51, 148.53, 147.23, 132.34, 130.23, 122.73, 121.06, 112.73, 21.73 ppm; LCMS: purity: 100%; RT: 4.726 (254  $\lambda$ ); *m/z*: 238.4 [M<sup>+</sup>].

4.1.12. 2-(5-Methylpyridin-2-yl)isoindoline-1,3-dione (**13**). Yield: 67%, mp: 166–170 °C. IR  $\nu_{\max}$  (KBr pellets): 3039.91 (CH stretch), 1736.38 (C=O) cm<sup>-1</sup>; <sup>1</sup>H NMR (400 MHz, DMSO-*d*<sub>6</sub>): 7.83–8.24 (m, 7H, Ar-H), 2.39 (s, 3H, CH<sub>3</sub>) ppm; <sup>13</sup>C NMR (DMSO-*d*<sub>6</sub>) 165.45, 152.48, 145.37, 137.54, 134.45, 132.12, 123.43, 123.50, 109.16, 18.40 ppm; LCMS: purity: 100%; RT: 4.853 (254  $\lambda$ ); *m/z*: 238.6 [M<sup>+</sup>].

4.1.13. 2-(5-Bromopyridin-2-yl)isoindoline-1,3-dione (**14**). Yield: 70%, mp: 162–166 °C. IR  $\nu_{\max}$  (KBr pellets): 3064.99 (CH stretch), 1718.63 (C=O), 715.61 (C-Br) cm<sup>-1</sup>; <sup>1</sup>H NMR (400 MHz, DMSO-*d*<sub>6</sub>): 7.55–8.79 (7H, Ar-H) ppm; <sup>13</sup>C NMR (DMSO-*d*<sub>6</sub>) 166.04, 150.08, 144.76, 141.20, 134.98, 131.26, 124.42, 123.70, 119.98 ppm; LCMS: purity: 100%; RT: 3.990 (254  $\lambda$ ); *m/z*: 303.1 [M<sup>+</sup>] and 305.2 [M + 2].

4.1.14. 5-(1,3-Dioxoisindolin-2-yl)-2-methylbenzoic Acid (**15**). Yield: 68%, mp: 240–248 °C. IR  $\nu_{\max}$  (KBr pellets): 3592.95 (OH stretch), 3077.53 (CH stretch), 1722.95 (C=O) cm<sup>-1</sup>; <sup>1</sup>H NMR (400 MHz, DMSO-*d*<sub>6</sub>): 11.12 (s, 1H, COOH), 6.98–8.30 (m, 7H, Ar-CH), 2.51 (s, 3H, CH<sub>3</sub>); <sup>13</sup>C NMR (DMSO-*d*<sub>6</sub>)  $\delta$  172.53, 168.24, 138.34, 134.34, 132.43, 132.24, 131.39, 129.66, 129.10, 123.23, 119.83, 22.12 ppm; LCMS: purity: 100%; RT: 5.625 (254  $\lambda$ ); *m/z*: 283.0 [M<sup>+</sup>].

4.1.15. 2-(5-(4-Methoxyphenyl)-1,3,4-thiadiazol-2-yl)isoindoline-1,3-dione (**16**). Yield: 69%, mp: 228–232 °C. IR  $\nu_{\max}$  (KBr pellets): 2987.90 (Aro. CH stretch), 2836.42 (Ali. CH stretch), 1702 (C=O cyclic amide) cm<sup>-1</sup>; <sup>1</sup>H NMR (400 MHz, DMSO-*d*<sub>6</sub>): 7.00–8.23 (m, 8H, Ar-CH), 3.84 (s, 1H, OCH<sub>3</sub>); <sup>13</sup>C NMR (DMSO-*d*<sub>6</sub>) 175.64, 173.42, 168.23, 160.62, 134.34, 132.24, 122.73, 128.45, 125.85, 114.83, 55.89 ppm; LCMS: purity: 100%; RT: 6.048 (254  $\lambda$ ); *m/z*: 337.4 [M<sup>+</sup>].

4.1.16. 2-(5-(4-Chorophenyl)-1,3,4-thiadiazol-2-yl)isoindoline-1,3-dione (**17**). Yield: 66%, mp: 272–280 °C. IR  $\nu_{\max}$  (KBr pellets): 2924.18 (CH stretch), 1774.00 (C=O cyclic amide), 757.09 (C-Cl) cm<sup>-1</sup>; <sup>1</sup>H NMR (400 MHz, DMSO-*d*<sub>6</sub>): 7.52–8.32 (m, 8H, Ar-CH); <sup>13</sup>C NMR (DMSO-

*d*<sub>6</sub>) 176.34, 174.63, 166.53, 135.42, 134.43, 132.24, 131.66, 124.73, 129.63, 128.29 ppm; LCMS: purity: 100%; RT: 6.550 (254  $\lambda$ ); *m/z*: 341.8 [M<sup>+</sup>] and 343.7 [M + 2].

4.1.17. 2-(5-(2-Chorophenyl)-1,3,4-thiadiazol-2-yl)isoindoline-1,3-dione (**18**). Yield: 68%, mp: 228–232 °C. IR  $\nu_{\max}$  (KBr pellets): 3024.13 (CH stretch), 1778.32 (C=O cyclic amide), 748.20 (C-Cl) cm<sup>-1</sup>; <sup>1</sup>H NMR (400 MHz, DMSO-*d*<sub>6</sub>): 7.30–8.24 (m, 8H, Ar-CH); <sup>13</sup>C NMR (DMSO-*d*<sub>6</sub>) 176.89, 174.78, 167.35, 136.92, 134.34, 132.24, 132.34, 130.12, 129.34, 128.79, 127.38, 124.24 ppm; LCMS: purity: 100%; RT: 6.354 (254  $\lambda$ ); *m/z*: 341.7 [M<sup>+</sup>] and 343.9 [M + 2].

4.1.18. 2-(5-(Phenyl)-1,3,4-thiadiazol-2-yl)isoindoline-1,3-dione (**19**). Yield: 74%, mp: 216–220 °C. IR  $\nu_{\max}$  (KBr pellets): 3152 (CH stretch), 1779.03 (C=O cyclic amide) cm<sup>-1</sup>; <sup>1</sup>H NMR (400 MHz, DMSO-*d*<sub>6</sub>): ppm 7.23–8.19 (m, 9H, Ar-CH); <sup>13</sup>C NMR (DMSO-*d*<sub>6</sub>) 174.12, 173.68, 166.24, 133.46, 133.65, 132.24, 130.12, 129.34, 128.23, 122.12 ppm; LCMS: purity: 95%; RT: 6.007 (254  $\lambda$ ); *m/z*: 307.5 [M<sup>+</sup>].

4.1.19. *N*-(1,3-Dioxoisindoline-2-yl)-4-hydroxybenzamide (**20**). Yield: 74%, mp: 288–299 °C. IR  $\nu_{\max}$  (KBr pellets): 3455.45 (OH stretch), 3054.38 (CH stretch), 1725.77 (C=O cyclic amide) cm<sup>-1</sup>; <sup>1</sup>H NMR (400 MHz, DMSO-*d*<sub>6</sub>): 11.21 (s, 1H, NH), 9.72 (s, 1H, OH), 6.80–8.01 (m, 8H, Ar-CH) ppm; <sup>13</sup>C NMR (DMSO-*d*<sub>6</sub>) 169.43, 164.18, 160.92, 134.24, 132.75, 128.29, 124.65, 124.73, 116.12 ppm; LCMS: purity: 94%; RT: 1.575 (254  $\lambda$ ); *m/z*: 282.6 [M<sup>+</sup>].

4.1.20. 2-(5-(3-Bromophenyl)-1,3,4-thiadiazol-2-yl)isoindoline-1,3-dione (**21**). Yield: 62%, mp: 292–294 °C. IR  $\nu_{\max}$  (KBr pellets): 2924.18 (CH stretch), 1767.80 (C=O cyclic amide), 712.72 (C-Br) cm<sup>-1</sup>; <sup>1</sup>H NMR (400 MHz, DMSO-*d*<sub>6</sub>): 7.43–8.25 (m, 8H, Ar-CH) ppm; <sup>13</sup>C NMR (DMSO-*d*<sub>6</sub>) 177.35, 174.60, 168.32, 135.74, 134.34, 132.24, 133.61, 131.47, 129.49, 128.61, 124.73, 122.32 ppm; LCMS: purity: 100%; RT: 6.648 (254  $\lambda$ ); *m/z*: 386.7 [M<sup>+</sup>] and 388.5 [M + 2].

4.1.21. 2-(5-(2-Methoxyphenyl)-1,3,4-thiadiazol-2-yl)isoindoline-1,3-dione (**22**). Yield: 69%, mp: 246–252 °C. IR  $\nu_{\max}$  (KBr pellets): 3031.90 (CH stretch), 1752.86 (C=O cyclic amide), 1252.81 (C-O) cm<sup>-1</sup>; <sup>1</sup>H NMR (400 MHz, DMSO-*d*<sub>6</sub>) ppm: 7.10–8.43 (m, 8H, Ar-CH), 3.92 (s, 1H, O-CH<sub>3</sub>); <sup>13</sup>C NMR (DMSO-*d*<sub>6</sub>) 174.14, 173.10, 167.43, 157.43, 135.45, 132.67, 129.12, 128.56, 122.73, 122.16, 121.65, 115.56 ppm; LCMS: purity: 100%; RT: 6.042 (254  $\lambda$ ); *m/z*: 337.6 [M<sup>+</sup>].

4.1.22. 2-(5-(*m*-Tolyl)-1,3,4-thiadiazol-2-yl)isoindoline-1,3-dione (**23**). Yield: 67%, mp: 148–150 °C. IR  $\nu_{\max}$  (KBr

pellets): 2923.22 (Aro. CH stretch), 2853.78 (Ali. CH stretch), 1767.80 (C=O cyclic amide)  $\text{cm}^{-1}$ ;  $^1\text{H}$  NMR (400 MHz, DMSO- $d_6$ ) ppm: 7.08–8.18 (m, 8H, Ar–CH), 2.51 (s, 1H, CH<sub>3</sub>);  $^{13}\text{C}$  NMR (DMSO- $d_6$ ) 172.43, 170.42, 165.12, 138.92, 132.34, 130.24, 133.34, 130.44, 129.51, 129.05, 127.93, 122.73, 21.46 ppm; LCMS: purity: 100%; RT: 6.408 (254  $\lambda$ );  $m/z$ : 321.6 [ $\text{M}^+$ ].

4.1.23. 2-(5-Benzyl-1,3,4-thiadiazol-2-yl)isoindoline-1,3-dione (**24**). Yield: 71%, mp: 176–184 °C. IR  $\nu_{\text{max}}$  (KBr pellets): 3005 (Aro. CH stretch), 2854.74 (Ali. CH stretch), 1727.67 (C=O cyclic amide)  $\text{cm}^{-1}$ ;  $^1\text{H}$  NMR (400 MHz, DMSO- $d_6$ ) ppm: 7.20–8.38 (m, 9H, Ar–CH), 3.86 (s, 1H, CH<sub>2</sub>);  $^{13}\text{C}$  NMR (DMSO- $d_6$ ) 172.34, 166.53, 160.80, 136.62, 135.34, 132.24, 129.60, 128.76, 125.87, 122.73 ppm; LCMS: purity: 100%; RT: 5.817 (254  $\lambda$ );  $m/z$ : 321.90 [ $\text{M}^+$ ].

4.1.24. 2-(5-(2-Fluorophenyl)-1,3,4-thiadiazol-2-yl)isoindoline-1,3-dione (**25**). Yield: 75%, mp: 222–232 °C. IR  $\nu_{\text{max}}$  (KBr pellets): 3089.71 (CH stretch), 1748.67 (C=O cyclic amide), 1219.05 (C–F)  $\text{cm}^{-1}$ ;  $^1\text{H}$  NMR (400 MHz, DMSO- $d_6$ ) 7.25–8.30 (m, 8H, Ar–CH) ppm;  $^{13}\text{C}$  NMR (DMSO- $d_6$ ) 174.54, 173.35, 167.74, 158.33, 138.34, 134.24, 130.31, 129.41, 124.82, 123.68, 123.34, 114.34 ppm; LCMS: purity: 95%; RT: 6.143 (254  $\lambda$ );  $m/z$ : 325.4 [ $\text{M}^+$ ].

4.1.25. 2-(5-(3-Chlorophenyl)-1,3,4-thiadiazol-2-yl)isoindoline-1,3-dione (**26**). Yield: 73%, mp: 242–250 °C. IR  $\nu_{\text{max}}$  (KBr pellets): 3124.00 (CH stretch), 1756.32 (C=O cyclic amide), 755.23 (C–Cl)  $\text{cm}^{-1}$ ;  $^1\text{H}$  NMR (400 MHz, DMSO- $d_6$ ) 7.12–8.19 (m, 8H, Ar–CH);  $^{13}\text{C}$  NMR (DMSO- $d_6$ ) 175.46, 173.45, 168.24, 134.29, 134.48, 134.34, 132.24, 129.55, 129.12, 128.26, 127.45, 122.12 ppm; LCMS: purity: 97%; RT: 6.545 (254  $\lambda$ );  $m/z$ : 341.8 [ $\text{M}^+$ ] and 343.9 [ $\text{M} + 2$ ].

4.1.26. 2-(5-(4-Iodophenyl)-1,3,4-thiadiazol-2-yl)isoindoline-1,3-dione (**27**). Yield: 78%, mp: 292–298 °C. IR  $\nu_{\text{max}}$  (KBr pellets): 2923.22 (CH stretch), 1749.91 (C=O cyclic amide), 693.43 (C–I)  $\text{cm}^{-1}$ ;  $^1\text{H}$  NMR (400 MHz, DMSO- $d_6$ ) 7.38–8.43 (m, 8H, Ar–CH);  $^{13}\text{C}$  NMR (DMSO- $d_6$ ) 176.34, 174.24, 167.12, 138.14, 134.34, 132.44, 132.24, 129.61, 123.78, 98.42 ppm; LCMS: purity: 100%; RT: 6.818 (254  $\lambda$ );  $m/z$ : 433.4 [ $\text{M}^+$ ].

4.1.27. 2-(5-(2-Nitrophenyl)-1,3,4-thiadiazol-2-yl)isoindoline-1,3-dione (**28**). Yield: 64%, mp: 232–238 °C. IR  $\nu_{\text{max}}$  (KBr pellets): 3096.82 (CH stretch), 1755.35 (C=O cyclic amide)  $\text{cm}^{-1}$ ;  $^1\text{H}$  NMR (400 MHz, DMSO- $d_6$ ) 7.14–8.12 (m, 8H, Ar–CH) ppm;  $^{13}\text{C}$  NMR (DMSO- $d_6$ ) 177.46, 174.35, 167.35, 146.92, 135.34, 134.54, 132.57, 131.63, 129.64, 128.54, 125.34, 124.42 ppm; LCMS: purity: 94%; RT: 5.775 (254  $\lambda$ );  $m/z$ : 352.4 [ $\text{M}^+$ ].

4.1.28. 2-(5-Methyl-1,3,4-thiadiazol-2-yl)isoindolin-1,3-dione (**29**). Yield: 74%, mp: 220–226 °C. IR  $\nu_{\text{max}}$  (KBr pellets): IR  $\nu_{\text{max}}$  (KBr pellets): 2981.08 (Aro. CH stretch), 2869.21 (Ali. CH stretch), 1769 (C=O cyclic amide)  $\text{cm}^{-1}$ ;  $^1\text{H}$  (400 MHz, DMSO- $d_6$ ): 7.61–8.14 (m, 4H, Ar–H), 2.42 (s, 3H, CH<sub>3</sub>) ppm;  $^{13}\text{C}$  NMR (DMSO- $d_6$ ) 172.53, 166.64, 142.37, 136.46, 132.24, 122.73, 19.10 ppm; LCMS: purity: 100%; RT: 4.120 (254  $\lambda$ );  $m/z$ : 245.3 [ $\text{M}^+$ ].

4.1.29. 2-(4-Methyl-2-oxo-2H-chromen-6-yl)isoindoline-1,3-dione (**30**). Yield: 72%, mp: 302–308 °C. IR  $\nu_{\text{max}}$  (KBr pellets): IR  $\nu_{\text{max}}$  (KBr pellets): 3232.12 (Aro. CH stretch), 2935.20 (Ali. CH stretch), 1725.17 (C=O cyclic amide)  $\text{cm}^{-1}$ ;  $^1\text{H}$  NMR (400 MHz, DMSO- $d_6$ ): 6.45–8.28 (m, 8H, Ar–H), 2.18 (s, 3H, CH<sub>3</sub>) ppm;  $^{13}\text{C}$  NMR (DMSO- $d_6$ ) 167.53, 160.58, 152.57, 149.15, 136.34, 132.10, 129.54, 127.74,

122.23, 121.25, 116.94, 116.44, 112.65, 18.64 ppm; LCMS: purity: 100%; RT: 5.642 (254  $\lambda$ );  $m/z$ : 305.9 [ $\text{M}^+$ ].

**4.2. Geometry Optimization.** The ground state (GS) of the tilted compound was optimized at the DFT level of theory using the hybrid functionals B3LYP in combination with the basis set 6-311\*\*.<sup>39,40</sup>

**4.3. DFT-Based Calculations of the Fourier Transform Infrared (FT-IR) and NMR Spectra.** A wide range of molecular properties can be predicted with DFT calculations, including equilibrium structure, charge distribution, FT-IR, and NMR spectral correlation. The hybrid functional B3LYP/6-311\*\* was used to derive the tilted compound's (compound **14**) FT-IR and NMR spectra. Using the GIAO approach, the predicted chemical shifts for  $^1\text{H}$  and  $^{13}\text{C}$  NMR have been calculated using the isotropic chemical shielding constants. The isotropic shielding constants were used to compute the isotropic chemical shifts,  $\delta_{\text{cal}}$ , in relation to tetramethylsilane (TMS).<sup>17,18</sup>

**4.4. Biological Activity.** **4.4.1. In Vitro Determination of Antimycobacterial Activity.** The *in vitro* antimycobacterial activity of synthesized compounds was determined as per the previously reported procedures.<sup>24–26</sup>

**4.4.2. Evaluation of In Vitro Cytotoxicity.** The cytotoxicity of compounds was calculated by monitoring THP-1 cell viability after 3 days in the existence of test compounds, as described in the report.<sup>24–26</sup>

**4.5. Docking Study.** The molecular docking Glide module (Schrodinger, Inc.) has been used for ligand docking against the Mtb *enoyl reductase* (InhA). The X-ray crystallographic structure of InhA protein cognate with 1-cyclohexyl-5-oxo-N-phenylpyrrolidine-3-carboxamide was retrieved from the Protein Databank, with accession ID 2H7I. The retrieved protein structure was prepared using the “protein preparation wizard” panel. Using prime during the stages of preprocessing, bond ordering was assigned, missing hydrogen was added, disulfide bonds were formed, and missing side chains and loops were modified. In the final refinement stage, the OPLS3 force field has been used to reach complete energetic optimization, with the RMSD of heavy atoms set to 0.3 Å. All synthesized isoindoline-1,3-dione derivatives (**2–30**), three-dimensional (3D) structures with relevant chiralities, were prepared with the LigPrep panel. The ionization state of each ligand structure was established at a physiological pH of  $7.2 \pm 0.2$ . By centralizing the cognate ligand in the crystal structure and using the default box dimension, the active side grid was assigned. Finally, the molecular docking study was carried out using Schrodinger's glide, in which the ready minimum-energy 3D structure of the ligands and the receptor grid file were loaded into Maestro's work area and the ligands were docked using standard precision (SP) docking methodology.<sup>41,42</sup>

**4.6. Binding Free Energy Calculation Using the Prime MMGBSA Approach.** The Schrodinger software's Prime module has been used to calculate the binding free energies of synthesized compounds in complex with Mtb InhA in terms of the MMGBSA method. The Prim measures the binding free energies of bound complexes using multiple nonpolar solvent-accessible surface area and executable van der Waals interactions, as well as advanced OPLS-2005 force field, nonpolar solvation, molecular mechanics, and polar solvation energies. A Glide pose viewer file of the docked complex was used for this calculation. The MMGBSA calculations are used to measure ligands' relative binding affinity to the target

receptor, and it infers that the stronger the binding affinity, the lower the value.<sup>41,42</sup>

**4.7. Density Functional Theory (DFT) Calculations.** DFT calculations were performed to determine the electronic molecular attributes, specifically the frontier molecular orbital (FMOs) density fields and molecular electrostatic maps, that can help to understand biological activity and molecular characteristics. The hybrid functional B3LYP/6-311G\*\* level has been used to compute the HOMO and LUMO of the synthesized compounds.<sup>39,40</sup> It also provides definitions of fundamental concepts about the stability and reactivity of molecular structures.<sup>39,40</sup> In quantum-chemical calculations, the energies of the FMOs, HOMO, and LUMO are accessible to deliver information about electron affinity (EA), ionization potential (IP), electrophilicity index ( $\omega$ ), electronegativity ( $\chi$ ), softness ( $s$ ), hardness ( $\eta$ ), and chemical potential ( $\mu$ ) to extrapolate the relationships among energy, structure, and reactivity characteristics of target materials.<sup>39,40</sup>

The IP and EA were calculated as follows

$$\text{IP} = -E_{\text{HOMO}} \quad \text{EA} = -E_{\text{LUMO}}$$

where  $E$  stands for energy

The global reactivity descriptors were calculated using Koopman's theorem,<sup>35</sup> which is represented by the equations below

$$\text{chemical potential } (\mu) = -(\text{IP} + \text{EA})/2$$

$$\text{hardness } (\eta) = (\text{IP} - \text{EA})/2$$

$$\text{softness}(s) = 1/2\eta$$

$$\text{electronegativity } (\chi) = (\text{IP} + \text{EA})/2$$

$$\text{global electrophilicity index } (\omega) = \mu^2/2\eta$$

**4.8. Molecular Dynamics Simulation.** The best docked conformation of compound **27** in complex with *Mtb InhA* has been further evaluated for thermodynamic behavior and stability using molecular dynamics simulation (MD).<sup>43</sup> The docked complex was solvated using a single point charge (SPC) as a water model. Proper counterions ( $\text{Na}^+$  and  $\text{Cl}^-$ ) and the orthorhombic cell were provided to achieve electro-neutrality in the system using Desmond's system builder.<sup>44</sup> The prepared system was minimized with a maximum of 2000 iterations and a gradient convergence cutoff of 1 kJ/mol. Before running the MD simulation, a six-stage NPT ( $N$  = number of atoms,  $P$  = pressure, and  $T$  = temperature) ensemble default relaxation procedure was executed.<sup>45</sup>

The ensemble was then submitted to a 100 ns molecular dynamics simulation, with snapshots taken every 100 ps. Finally, the ligand–protein complex binding confirmation and stability from MD trajectories were analyzed using Desmond's simulation interaction diagram (SID).<sup>45</sup> The binding free energy of the receptor and ligand during simulation is computed by the python script thermal mmgsa.py. The average binding free energy was calculated using the 0–100 ns MD simulation trajectory as input during the MMGSA calculation.<sup>43–45</sup>

**4.9. InhA Inhibition Assay.** The InhA inhibition assay was performed as per the reported protocol.<sup>46</sup> In short, stock solutions of compound **27** were formulated in DMSO so that the final concentration of this co-solvent was constant at 5% v/v for all kinetic reactions at a final volume of 1 mL. As previously described, kinetic assays were implemented employ-

ing *trans*-2-dodecenoyl-coenzyme A (DDCoA) and wild-type InhA. Reactions were performed at 25 °C in an aqueous buffer (30 mM PIPES and 150 mM NaCl pH 6.8) containing an additional 250  $\mu\text{M}$  cofactor (NADH), a 50  $\mu\text{M}$  substrate (DDCoA), and a compound tested. Reactions began with the addition of InhA (100 nM final) and NADH oxidation followed at 340 nm. Triclosan has been used as a positive control device.

## ■ ASSOCIATED CONTENT

### Supporting Information

The Supporting Information is available free of charge at <https://pubs.acs.org/doi/10.1021/acsomega.2c01981>.

LCMS of compounds **2–11**, **14**, **15**, **21**, **24**, and **30** and per residue binding free energy during 100 ns time (Table 1S) (PDF)

## ■ AUTHOR INFORMATION

### Corresponding Author

Harun Patel – Division of Computer-Aided Drug Design, Department of Pharmaceutical Chemistry, R. C. Patel Institute of Pharmaceutical Education and Research, Shirpur 425405 Maharashtra, India; [orcid.org/0000-0003-0920-1266](https://orcid.org/0000-0003-0920-1266); Email: [hpatel\\_38@yahoo.com](mailto:hpatel_38@yahoo.com)

### Authors

Iqrar Ahmad – Division of Computer-Aided Drug Design, Department of Pharmaceutical Chemistry, R. C. Patel Institute of Pharmaceutical Education and Research, Shirpur 425405 Maharashtra, India

Rahul H. Pawara – Division of Computer-Aided Drug Design, Department of Pharmaceutical Chemistry, R. C. Patel Institute of Pharmaceutical Education and Research, Shirpur 425405 Maharashtra, India

Rukaiyya T. Girase – Division of Computer-Aided Drug Design, Department of Pharmaceutical Chemistry, R. C. Patel Institute of Pharmaceutical Education and Research, Shirpur 425405 Maharashtra, India

Asama Y. Pathan – Division of Computer-Aided Drug Design, Department of Pharmaceutical Chemistry, R. C. Patel Institute of Pharmaceutical Education and Research, Shirpur 425405 Maharashtra, India

Vilas R. Jagatap – Division of Computer-Aided Drug Design, Department of Pharmaceutical Chemistry, R. C. Patel Institute of Pharmaceutical Education and Research, Shirpur 425405 Maharashtra, India

Nisheeth Desai – Division of Medicinal Chemistry, Department of Chemistry (DST-FIST Sponsored), Maharaja Krishnakumarsinhji Bhavnagar University, Bhavnagar 364002, India; [orcid.org/0000-0001-6864-8661](https://orcid.org/0000-0001-6864-8661)

Yusuf Oloruntoyin Ayipo – Centre for Drug Research, Universiti Sains Malaysia, USM, 11800 Gelugor, Pulau Pinang, Malaysia; [orcid.org/0000-0001-5951-9788](https://orcid.org/0000-0001-5951-9788)

Sanjay J. Surana – Division of Computer-Aided Drug Design, Department of Pharmaceutical Chemistry, R. C. Patel Institute of Pharmaceutical Education and Research, Shirpur 425405 Maharashtra, India

Complete contact information is available at:

<https://pubs.acs.org/doi/10.1021/acsomega.2c01981>

### Notes

The authors declare no competing financial interest.

## ACKNOWLEDGMENTS

The authors thank the Indian Council of Medical Research (ICMR)—Government of India (Grant ISRM/12 (11)/2019) for funding the project. N.D. is thankful to the University Grants Commission, New Delhi, for awarding the BSR Faculty Fellowship 2019 (F18-1/2011, BSR) and financial assistance.

## REFERENCES

- (1) World Health Organization. *Tuberculosis*. <https://www.who.int/news-room/fact-sheets/detail/tuberculosis> (accessed 2022-04-01).
- (2) MacNeil, A.; Glaziou, P.; Sismanidis, C.; Maloney, S.; Floyd, K. Global Epidemiology of Tuberculosis and Progress Toward Achieving Global Targets - 2017. *Morb. Mortal. Wkly. Rep.* **2019**, *68*, 263–266.
- (3) Shinde, Y.; Ahmad, I.; Surana, S.; Patel, H. The Mur Enzymes Chink in the Armour of *Mycobacterium tuberculosis* cell wall. *Eur. J. Med. Chem.* **2021**, *222*, No. 113568.
- (4) Chakraborty, S.; Rhee, K. Y. Tuberculosis Drug Development: History and Evolution of the Mechanism-Based Paradigm. *Cold Spring Harbor Perspect. Med.* **2015**, *5*, No. a021147.
- (5) Sotgiu, G.; Centis, R.; D'ambrosio, L.; Migliori, G. B. Tuberculosis treatment and drug regimens. *Cold Spring Harbor Perspect. Med.* **2015**, *5*, No. a017822.
- (6) Andries, K.; Verhasselt, P.; Guillemont, J.; Göhlmann, H. W.; Neefs, J. M.; Winkler, H.; Van Gestel, J.; Timmerman, P.; Zhu, M.; Lee, E.; Williams, P.; de Chaffoy, D.; Huitric, E.; Hoffner, S.; Cambau, E.; Truffot-Pernot, C.; Lounis, N.; Jarlier, V. A diarylquinoline drug active on the ATP synthase of *Mycobacterium tuberculosis*. *Science* **2005**, *307*, 223–227.
- (7) Alffenaar, J. W.; van Altena, R.; Harmelink, I. M.; Filguera, P.; Molenaar, E.; Wessels, A. M.; van Soolingen, D.; Kosterink, J. G.; Uges, D. R.; van der Werf, T. S. Comparison of the pharmacokinetics of two dosage regimens of linezolid in multidrug-resistant and extensively drug-resistant tuberculosis patients. *Clin. Pharmacokinet.* **2010**, *49*, 559–565.
- (8) Arentz, M.; Pavlinac, P.; Kimerling, M. E.; Horne, D. J.; Falzon, D.; Schünemann, H. J.; Royce, S.; Dheda, K.; Watson, J. L. ART study group. Use of anti-retroviral therapy in tuberculosis patients on second-line anti-TB regimens: a systematic review. *PLoS One* **2012**, *7*, No. e47370.
- (9) Akgün, H.; Karamelkoğlu, I.; Berk, B.; Kurnaz, I.; Sarıbiyık, G.; Oktem, S.; Kocagöz, T. Synthesis and antimycobacterial activity of some phthalimide derivatives. *Bioorg. Med. Chem.* **2012**, *20*, 4149–4154.
- (10) Othman, I. M. M.; Gad-Elkareem, M. A. M.; El-Naggar, M.; Nossier, E. S.; Amr, A. E. E. Novel phthalimide based analogues: design, synthesis, biological evaluation, and molecular docking studies. *J. Enzyme Inhib. Med. Chem.* **2019**, *34*, 1259–1270.
- (11) Arif, R.; Pattan, S. N.; Ansari, I. A.; Shahid, M.; Irfan, M.; Alam, S.; Abid, M.; Rahisuddin. Synthesis, molecular docking and DNA binding studies of phthalimide- based cop per(II) complex: In vitro antibacterial, hemolytic and antioxidant assessment. *J. Mol. Struct.* **2018**, *1160*, 142–153.
- (12) Orzeszko, A.; Kamińska, B.; Orzeszko, G.; Starościk, B. J. Synthesis and antimicrobial activity of new adamantane derivatives. *II Farmaco* **2000**, *55*, 619–623.
- (13) Elumalai, K.; Ali, M. A.; Elumalai, M.; Eluri, K.; Srinivasan, S.; Srinivasan, S.; Mohanthic, S. K. Synthesis, characterization and biological evaluation of acetazolamide, cycloserine and isoniazid condensed some novel phthalimide derivatives. *Int. J. Chem. Anal. Sci.* **2013**, *4*, 57–61.
- (14) Phatak, P. S.; Bakale, R. D.; Dhupal, S. T.; Dahiwade, L. K.; Choudhari, P. B.; Krishna, V. S.; Sriram, D.; Haval, K. P. Synthesis, antitubercular evaluation and molecular docking studies of phthalimide bearing 1,2,3-triazoles. *Synth. Commun.* **2019**, *49*, 2017–2028.
- (15) Paraiso, W. K.; Alea, G. Synthesis and in vitro antimycobacterial activity determination of phthalimide derivatives. *Manila J. Sci.* **2013**, *8*, 27–34.
- (16) Santos, J. L.; Yamasaki, P. R.; Chin, C. M.; Takashi, C. H.; Pavan, F. R.; Leite, C. Q. Synthesis and in vitro anti *Mycobacterium tuberculosis* activity of a series of phthalimide derivatives. *Bioorg. Med. Chem.* **2009**, *17*, 3795–3799.
- (17) Jiang, S.; Jin, Y.; Yan, R.; Wang, Z. Detailed structural study of cyclic anticancer drug Lorlatinib: spectroscopic and stereostructure investigation (IR, ECD and NMR) using density functional theory approach. *J. Mol. Struct.* **2021**, *1225*, No. 129295.
- (18) Salihović, M.; Pazalja, M.; Halilovic, S. S.; Veljovic, E.; Mahmutovic-Dizdarevi, I.; Roca, S.; Novakovic, I.; Trifunovic, S. Synthesis, characterization, antimicrobial activity and DFT study of some novel Schiff bases. *J. Mol. Struct.* **2021**, *1241*, No. 130670.
- (19) Hesterkamp, T.; Barker, J.; Davenport, A.; Whittaker, M. Fragment based drug discovery using fluorescence correlation: spectroscopy techniques: challenges and solutions. *Curr. Top. Med. Chem.* **2007**, *7*, 1582–1591.
- (20) Clark, J. *High Resolution Proton NMR Spectra*. [https://chem.libretexts.org/Bookshelves/Physical\\_and\\_Theoretical\\_Chemistry\\_Textbook\\_Maps/Supplemental\\_Modules\\_\(Physical\\_and\\_Theoretical\\_Chemistry\)/Spectroscopy/Magnetic\\_Resonance\\_Spectroscopies/Nuclear\\_Magnetic\\_Resonance/NMR%3A\\_Structural\\_Assignment/High\\_Resolution\\_Proton\\_NMR\\_Spectra](https://chem.libretexts.org/Bookshelves/Physical_and_Theoretical_Chemistry_Textbook_Maps/Supplemental_Modules_(Physical_and_Theoretical_Chemistry)/Spectroscopy/Magnetic_Resonance_Spectroscopies/Nuclear_Magnetic_Resonance/NMR%3A_Structural_Assignment/High_Resolution_Proton_NMR_Spectra) (accessed 2022-04-01).
- (21) Muthu, S.; Porchelvi, E. E. FTIR, FT-RAMAN, NMR, spectra, normal co-ordinate analysis, NBO, NLO and DFT calculation of *N,N*-diethyl-4-methylpiperazine-1-carboxamide molecule. *Spectrochim. Acta, Part A* **2013**, *115*, 275–286.
- (22) Muthu, S.; Ramachandran, G. Spectroscopic studies (FTIR, FT-Raman and UV-Visible), normal coordinate analysis, NBO analysis, first order hyper polarizability, HOMO and LUMO analysis of (1*R*)-*N*-(Prop-2-yn-1-yl)-2,3-dihydro-1*H*-inden-1-amine molecule by ab initio HF and density functional methods. *Spectrochim. Acta, Part A* **2014**, *121*, 394–403.
- (23) Mathammal, R.; Monisha, N. R.; Yasaswini, S.; Krishnakumar, V. Molecular structure, vibrational analysis (FT-IR, FT-Raman), NMR, UV, NBO and HOMO-LUMO analysis of *N,N*-Diphenyl Formamide based on DFT calculations. *Spectrochim. Acta, Part A* **2015**, *139*, 521–532.
- (24) Karunanidhi, S.; Chandrasekaran, B.; Karpoornath, R.; Patel, H. M.; Kayamba, F.; Merugu, S. R.; Kumar, V.; Dhawan, S.; Kushwaha, B.; Mahlalela, M. C. Novel thiomorpholine tethered isatin hydrazones as potential inhibitors of resistant *Mycobacterium tuberculosis*. *Bioorg. Chem.* **2021**, *115*, No. 105133.
- (25) Patel, H. M.; Palkar, M.; Karpoornath, R. Exploring MDR-TB Inhibitory Potential of 4-Aminoquinazolines as *Mycobacterium tuberculosis* *N*-Acetylglucosamine-1-Phosphate Uridyltransferase (GlmU<sup>MTB</sup>) Inhibitors. *Chem. Biodiversity* **2020**, *17*, No. e2000237.
- (26) Patel, H.; Chaudhari, K.; Jain, P.; Surana, S. Synthesis and in vitro antitubercular activity of pyridine analogues against the resistant *Mycobacterium tuberculosis*. *Bioorg. Chem.* **2020**, *102*, No. 104099.
- (27) Takayama, K.; Wang, C.; Besra, G. S. Pathway to synthesis and processing of mycolic acids in *Mycobacterium tuberculosis*. *Clin. Microbiol. Rev.* **2005**, *18*, 81–101.
- (28) Patel, H.; Ahmad, I.; Jadhav, H.; Pawara, R.; Lokwani, D.; Surana, S. Investigating the Impact of Different Acrylamide (Electrophilic Warhead) on Osimertinib's Pharmacological Spectrum by Molecular Mechanic and Quantum Mechanic Approach. *Comb. Chem. High Throughput Screening* **2021**, *25*, 149–166.
- (29) Salihović, M.; Pazalja, M.; Halilovic, S. S.; Veljovic, E.; Mahmutovic-Dizdarevi, I.; Roca, S.; Novakovic, I.; Trifunovic, S. Synthesis, characterization, antimicrobial activity and DFT study of some novel Schiff bases. *J. Mol. Struct.* **2021**, *1241*, No. 130670.
- (30) Jiang, S.; Jin, Y.; Yan, R.; Wang, Z. Detailed structural study of cyclic anticancer drug Lorlatinib: spectroscopic and stereostructure investigation (IR, ECD and NMR) using density functional theory approach. *J. Mol. Struct.* **2021**, *1225*, No. 129295.
- (31) Salihović, M.; Pazalja, M.; Halilovic, S. S.; Veljovic, E.; Mahmutovic-Dizdarevi, I.; Roca, S.; Novakovic, I.; Trifunovic, S.



Synthesis, characterization, antimicrobial activity and DFT study of some novel Schiff bases. *J. Mol. Struct.* **2021**, *1241*, No. 130670.

(32) Khalid, M.; Ullah, M. A.; Adeel, M.; Khan, M. U.; Tahir, M. N.; Braga, A. A. C. Synthesis, crystal structure analysis, spectral IR, UV–Vis, NMR assessments, electronic and nonlinear optical properties of potent quinoline based derivatives: Interplay of experimental and DFT study. *J. Saudi Chem. Soc.* **2019**, *23*, 546–560.

(33) Qi, L.; Li, M. C.; Bai, J. C.; Ren, Y. H.; Ma, H. X. *In vitro* antifungal activities, molecular docking, and DFT studies of 4-amine-3-hydrazino-5-mercapto-1,2,4-triazole derivatives. *Bioorg. Med. Chem. Lett.* **2021**, *40*, No. 127902.

(34) Choudhary, V. K.; Bhatt, A. K.; Dash, D.; Sharma, N. DFT calculations on molecular structures, HOMO–LUMO study, reactivity descriptors and spectral analyses of newly synthesized diorganotin(IV) 2-chloridophenylacetohydroxamate complexes. *J. Comput. Chem.* **2019**, *40*, 2354–2363.

(35) Govindarajan, M.; Karabacak, M.; Periandy, S.; Tanuja, D. Spectroscopic (FT-IR, FT-Raman, UV and NMR) investigation and NLO, HOMO-LUMO, NBO analysis of organic 2,4,5-trichloroaniline. *Spectrochim. Acta, Part A* **2012**, *97*, 231–245.

(36) Ahmad, I.; Akand, S. R.; Shaikh, M.; Pawara, R.; Manjula, S. N.; Patel, H. Synthesis, molecular modelling study of the methaqualone analogues as anti-convulsant agent with improved cognition activity and minimized neurotoxicity. *J. Mol. Struct.* **2022**, *1251*, No. 131972.

(37) Pawara, R.; Ahmad, I.; Nayak, D.; Wagh, S.; Wadkar, A.; Ansari, A.; Belamkar, S.; Surana, S.; Kundu, C. N.; Patil, C.; Patel, H. Novel, selective acrylamide linked quinazolines for the treatment of double mutant EGFR-L858R/T790M Non-Small-Cell lung cancer (NSCLC). *Bioorg. Chem.* **2021**, *115*, No. 105234.

(38) Ayipo, Y. O.; Yahaya, S. N.; Babamale, H. F.; Ahmad, I.; Patel, H.; Mordi, M. N.  $\beta$ -Carboline alkaloids induce structural plasticity and inhibition of SARS-CoV-2 nsp3 macrodomain more potently than remdesivir metabolite GS-441524: computational approach. *Turk. J. Biol.* **2021**, *45*, 503–517.

(39) Momany, F. A.; Appell, M.; Willett, J. L.; Bosma, W. B. B3LYP/6-311++G\*\* geometry-optimization study of pentahydrates of  $\alpha$ - and  $\beta$ -D-glucopyranose. *Carbohydr. Res.* **2005**, *340*, 1638–1655.

(40) Appell, M.; Willett, J. L.; Momany, F. A. DFT study of alpha- and beta-D-mannopyranose at the B3LYP/6-311++G\*\* level. *Carbohydr. Res.* **2005**, *340*, 459–468.

(41) Pawara, R.; Ahmad, I.; Surana, S.; Patel, H. Computational identification of 2,4-disubstituted amino-pyrimidines as L858R/T790M-EGFR double mutant inhibitors using pharmacophore mapping, molecular docking, binding free energy calculation, DFT study and molecular dynamic simulation. *In Silico Pharmacol.* **2021**, *9*, No. 54.

(42) Ahmad, I.; Jadhav, H.; Shinde, Y.; Jagtap, V.; Girase, R.; Patel, H. Optimizing Bedaquiline for cardiotoxicity by structure based virtual screening, DFT analysis and molecular dynamic simulation studies to identify selective MDR-TB inhibitors. *In Silico Pharmacol.* **2021**, *9*, No. 23.

(43) Patel, H.; Pawara, R.; Pawara, K.; Ahmed, F.; Shirkhedkar, A.; Surana, S. A structural insight of bedaquiline for the cardiotoxicity and hepatotoxicity. *Tuberculosis* **2019**, *117*, 79–84.

(44) Lee, H. Y.; Cho, D. Y.; Ahmad, I.; Patel, H. M.; Kim, M. J.; Jung, J. G.; Jeong, E. H.; Haque, M. A.; Cho, K. M. Mining of a novel esterase (est3S) gene from a cow rumen metagenomic library with organosphosphorus insecticides degrading capability: Catalytic insights by site directed mutations, docking, and molecular dynamic simulations. *Int. J. Biol. Macromol.* **2021**, *190*, 441–455.

(45) Ahmad, I.; Kumar, D.; Patel, H. Computational investigation of phytochemicals from *Withania somnifera* (Indian ginseng/ashwagandha) as plausible inhibitors of GluN2B-containing NMDA receptors. *J. Biomol. Struct. Dyn.* **2021**, *10*, 1–13.

(46) Chollet, A.; Mori, G.; Menendez, C.; Rodriguez, F.; Fabing, I.; Pasca, M. R.; Madacki, J.; Kordulakova, J.; Constant, P.; Quemard, A.; Bernardes-Génisson, V.; Lherbet, C.; Baltas, M. Design, synthesis and evaluation of new GEQ derivatives as inhibitors of InhA enzyme and

*Mycobacterium tuberculosis* growth. *Eur. J. Med. Chem.* **2015**, *101*, 218–235.